



Full length article

## Sources of PM<sub>2.5</sub> exposure and health benefits of clean air actions in Shanghai

Yixuan Gu<sup>a,b,c,\*</sup>, Daven K. Henze<sup>b</sup>, Hong Liao<sup>a</sup>

<sup>a</sup> Jiangsu Key Laboratory of Atmospheric Environment Monitoring and Pollution Control, Collaborative Innovation Center of Atmospheric Environment and Equipment Technology, Joint International Research Laboratory of Climate and Environment Change, School of Environmental Science and Engineering, Nanjing University of Information Science and Technology, Nanjing 210044, China

<sup>b</sup> Department of Mechanical Engineering, University of Colorado, Boulder, CO 80309, USA

<sup>c</sup> Shanghai Typhoon Institute, China Meteorological Administration, Shanghai 200030, China

## ARTICLE INFO

Handling Editor: Dr. Hanna Boogaard

## Keywords:

Urban PM<sub>2.5</sub> pollution  
Health impacts  
Source apportionment  
Adjoint modeling  
Emission control  
Urban health

## ABSTRACT

Estimating PM<sub>2.5</sub> exposure and its health impacts in cities involves large uncertainty due to the limitations of model resolutions. Consequently, attributing the sources of PM<sub>2.5</sub>-related health impacts at the city level remains challenging. We characterize the health impacts associated with chronic PM<sub>2.5</sub> exposure and anthropogenic emissions in Shanghai using a chemical transport model (GEOS-Chem) and its adjoint. By incorporating high-resolution satellited-derived PM<sub>2.5</sub> estimates into the calculation, we investigate the response of PM<sub>2.5</sub> exposure and its related health impacts in Shanghai to changes in anthropogenic emissions from each individual region, species, sector, and month. We estimate that a 10% decrease in anthropogenic emissions throughout China avoids over 752 (506–1,044) PM<sub>2.5</sub>-related premature deaths in Shanghai, with changes in local emissions potentially saving 241 (161–334) lives. Ammonia (NH<sub>3</sub>) emissions are identified as the marginal dominant contributor to the health impacts due to the NH<sub>3</sub>-limited PM<sub>2.5</sub> formation within the city, thus controlling NH<sub>3</sub> emissions at both the local and regional scales are effective at reducing the population's exposure to PM<sub>2.5</sub>. A negative response of the PM<sub>2.5</sub> exposure to local nitrogen oxides (NO<sub>x</sub>) emission changes is detected in winter. Even so, controlling NO<sub>x</sub> emissions is still justified since the negative impacts decrease as anthropogenic emissions decline and NO<sub>x</sub> emission reductions benefit the public health on average. The anthropogenic emission changes due to Clean Air Actions helped avoid 3,132 (2,108–4,346) PM<sub>2.5</sub>-related premature deaths in 2019 relative to 2013, most of which are associated with emission reductions in the agricultural and industrial sectors.

### 1. Introduction

Long-term exposure to ambient fine particulate matter (particles with an aerodynamic diameter smaller than 2.5 μm; PM<sub>2.5</sub>) causes increased risk of premature death due to respiratory and cardiovascular diseases, and lung cancer, resulting in a significant health burden globally (Lelieveld et al., 2015; Burnett et al., 2018; Murray et al., 2020). The Global Burden of Disease (GBD) 2015 study shows that chronic PM<sub>2.5</sub> exposure has caused 4.2 million premature deaths worldwide (Cohen et al., 2017). Notably, China accounts for over a quarter of these premature deaths and is one of the most significantly affected countries in terms of the health risks posed by PM<sub>2.5</sub> exposure (IHME, 2018). In densely populated urban areas, the PM<sub>2.5</sub>-related health risk is much

higher than those in rural areas. In 2014, for example, the observed PM<sub>2.5</sub> concentrations in dense urban areas were 1.1–2.1 times those in rural areas in China, causing 85–225 more premature deaths per square kilometer in dense urban areas than rural areas (Lu et al., 2019). In addition to regional and nation-level actions, cities are thus responsible for developing effective and informed pollution control strategies to mitigate the adverse health impacts associated with PM<sub>2.5</sub>, which is a pressing sustainability challenge confronting China.

Shanghai is a highly urbanized city in China, with a population of 24.76 million and an urbanization rate of 89.3 % in 2022 (Shanghai Municipal Bureau of Statistics, 2023). Even though a series of Clean Air Actions have been implemented to reduce PM<sub>2.5</sub> concentrations since 2013 (Shi et al., 2021; Liu et al., 2022; Ali et al., 2023), health problems

\* Corresponding author at: Jiangsu Key Laboratory of Atmospheric Environment Monitoring and Pollution Control, Jiangsu Collaborative Innovation Center of Atmospheric Environment and Equipment Technology, School of Environmental Science and Engineering, Nanjing University of Information Science & Technology, Nanjing 210044, China.

E-mail address: [yixuan.gu@nuist.edu.cn](mailto:yixuan.gu@nuist.edu.cn) (Y. Gu).

<https://doi.org/10.1016/j.envint.2025.109259>

Received 29 October 2024; Received in revised form 20 December 2024; Accepted 7 January 2025

Available online 7 January 2025

0160-4120/© 2025 The Authors. Published by Elsevier Ltd. This is an open access article under the CC BY-NC license (<http://creativecommons.org/licenses/by-nc/4.0/>).

attributable to PM<sub>2.5</sub> exposure remain significant. In 2023, the annual mean PM<sub>2.5</sub> concentration was 28.7  $\mu\text{g m}^{-3}$  in Shanghai (IQAir, 2023), which is approximately 5.7 times higher than the Air Quality Guideline (AQG, 5  $\mu\text{g m}^{-3}$ ) established by the World Health Organization (WHO). Chronic PM<sub>2.5</sub> exposure in Shanghai in 2016 is estimated to have caused 10,418–20,762 premature deaths, which makes the city one of the most at-risk cities in China in terms of PM<sub>2.5</sub>-related health impacts (Zheng et al., 2021). Despite improvements in air quality, the rate at which PM<sub>2.5</sub> concentrations have decreased has slowed as the PM<sub>2.5</sub> concentrations themselves have come down (Xiao et al., 2022), suggesting that more effective and accurate control strategies are needed to make further progress.

To facilitate effective emission reductions, ongoing efforts are being made to track the sources of PM<sub>2.5</sub> pollution in China. Observational studies use classification approaches, for example positive matrix factorization, to identify the sources of aerosol based on measurements of species concentrations from various source types (e.g., Li et al., 2020; Feng et al., 2022). Model studies typically track emissions from aggregated types of sources by perturbing or tagging emissions from specific source categories (e.g., Li et al., 2016a; Gu et al., 2021; Ping et al., 2023). The applicability of both approaches is limited by computational costs, so they identify only a limited number of predefined sectoral and regional sources during a single time period. In contrast, adjoint model-based sensitivity analysis provides an alternative approach to efficiently calculate the response of a pollutant exposure metric to a large number (e.g.,  $>10^4$ ) of sources (Hakami et al., 2007; Henze et al., 2007, 2009). However, characterizing urban-scale health impacts remains challenging. The urban-scale spatial variability of PM<sub>2.5</sub> exposure is difficult to capture with model simulations, as the model domain needs to be large enough to capture all upwind sources and the model needs to be run on annual time scales, meaning the models are necessarily coarse, spatially. This can result in large uncertainties in estimating health impacts (Punger and West, 2013; Li et al., 2016b). Recent adjoint source apportionment studies have incorporated satellite-derived surface PM<sub>2.5</sub> products into the model, by which the PM<sub>2.5</sub> exposure is refined at the neighborhood scale (Nawaz and Henze, 2020; Nawaz et al., 2021; Gu et al., 2023a), although these updated adjoint studies have been conducted without a focus yet on Chinese cities.

In China, previous studies applying the adjoint method to identify sources of PM<sub>2.5</sub> concentrations have primarily focused on severe air pollution episodes or polluted seasons (e.g., Mao et al., 2020; Wang et al., 2022; Zhang et al., 2015, 2016; Hu et al., 2024). Adjoint-based analysis of health impacts attributable to PM<sub>2.5</sub> exposure in specific cities in China remains limited. Using the nested-grid capability of the GEOS-Chem adjoint model, Zhao et al. (2019) calculated the sensitivities of PM<sub>2.5</sub>-related premature deaths in seven receptor regions to emissions of all species, locations, and times in China. However, the model resolution of this country-level study was approximately 50 km, which may be too coarse to investigate city-level characteristics. Additionally, secondary organic aerosols (SOA) from anthropogenic volatile organic compounds (VOCs) have not been included in many adjoint-based source attribution studies, leading to potential gaps in identifying SOA-related sources when designing effective emission control strategies.

In this study, we address the challenges identified above by applying the GEOS-Chem adjoint model to investigate the response of city-level PM<sub>2.5</sub>-related health impacts to various emission changes in Shanghai. The response of PM<sub>2.5</sub>-related premature deaths in Shanghai to anthropogenic emission changes from each individual species, sector, and province is quantified on a monthly scale. Satellite-derived surface PM<sub>2.5</sub> concentrations are incorporated into the adjoint sensitivity calculation to improve the model's estimate of PM<sub>2.5</sub> exposure in the city. The contribution of SOA from anthropogenic VOCs is included. To investigate the effectiveness of the Clean Air Actions, changes in the response of PM<sub>2.5</sub> exposure to various emission changes are investigated from 2013 to 2019. The objective is to provide detailed health burden

source characterization to enhance the city's ability for addressing air pollution and its related health damages.

## 2. Methods

### 2.1. The GEOS-Chem model

We use the nested-grid capability of the chemical transport model GEOS-Chem (aka forward model) to simulate concentrations of air pollutants at the  $0.25^\circ \times 0.3125^\circ$  horizontal resolution over the East Asia domain ( $100^\circ$ – $140^\circ\text{E}$ ,  $20^\circ$ – $50^\circ\text{N}$ ). The forward model is included in the adjoint model version 35n (Henze et al., 2007), driven by assimilated meteorological fields from the Goddard Earth Observing System (GEOS-FP) of the NASA Global Modeling and Assimilation Office. A new SOA scheme has been incorporated into the model following Nault et al. (2021) and Nawaz et al. (2021). PM<sub>2.5</sub> concentration is thus calculated as the total mass of aerosol-phase sulfate ( $\text{SO}_4^{2-}$ ), nitrate ( $\text{NO}_3^-$ ), ammonium ( $\text{NH}_4^+$ ), black carbon (BC), primary organic mass (POM), SOA, fine mode mineral dust (aerodynamic diameter  $< 1.8 \mu\text{m}$ ), and associated water at 35 % RH and standard temperature and pressure. POM concentrations are estimated by multiplying the concentrations of primary organic carbon (OC) to satellite-derived POM/OC ratios by season and grid cell (Philip et al., 2014). Chemical boundary conditions, which are updated every 3 h, are from a global simulation at a horizontal resolution of  $2^\circ \times 2.5^\circ$  and a nested simulation at the  $0.25^\circ \times 0.3125^\circ$  horizontal resolution over a larger Asian domain ( $70^\circ$ – $140^\circ\text{E}$ ,  $15^\circ$ – $55^\circ\text{N}$ ). The model domains are shown in Fig. 1. We conduct a 6-month spin up and one-year continuous simulation to generate restart files for the base simulation in 2019 over the East Asia domain.

The Multi-resolution Emission Inventory for China (MEIC, version 1.4, <https://www.meicmodel.org>, last access: 29 March 2024) is used to simulate aerosol concentrations in mainland China. The MEIC inventory, with a horizontal resolution of  $0.25^\circ \times 0.25^\circ$ , provides emissions of sulfur dioxides ( $\text{SO}_2$ ), nitrogen oxides ( $\text{NO}_x$ ), carbon monoxide (CO), nonmethane volatile organic compounds (NMVOCs), ammonia ( $\text{NH}_3$ ), OC, BC, and PM<sub>2.5</sub> across five sectors (i.e., power, industry, residential, transportation, and agriculture) on a monthly scale. Anthropogenic emissions outside mainland China are from the Hemispheric Transport of Air Pollution version 3 (HTAPv3, [https://edgar.jrc.ec.europa.eu/data\\_set\\_htap\\_v3](https://edgar.jrc.ec.europa.eu/data_set_htap_v3), last access: 29 March 2024) anthropogenic emission inventory, with a horizontal resolution of  $0.1^\circ \times 0.1^\circ$ . The calculation of emissions of anthropogenic SOA precursors (SOAP) and the speciation of NMVOC emissions are described in our previous work (Gu et al., 2023a). The total NMVOCs emissions in every grid box are distributed to individual species emissions according to the speciation information from the NMVOC EDGARv4.3.2 database (Huang et al., 2017). SOAP represents the lumped precursors of anthropogenic SOA including aromatics and intermediate-volatile organic compounds (IVOCs) and semi-volatile organic compounds (SVOCs). IVOCs generally have a  $C^*$  of 103 to 106  $\mu\text{g m}^{-3}$  and SVOCs have a  $C^*$  of 1 to 102  $\mu\text{g m}^{-3}$  (Nault et al., 2021). Natural emissions, including those from biogenic (Guenther et al., 2006), biomass burning (Van Der Werf et al., 2010), dust (Zender et al., 2003), lightning (Murray et al., 2012), and soil sources (Hudman et al., 2012), are included in the model calculation.

### 2.2. Adjoint sensitivity calculation

For our source apportionment in the base simulation, we conduct 12 monthly adjoint simulations in 2019 over the East Asia domain, and force the adjoint after each forward model run to calculate the sensitivity of the receptor function ( $J$ ), defined as the annual mean population-weighted PM<sub>2.5</sub> concentration in Shanghai, to changes in emissions of major PM<sub>2.5</sub> precursors (i.e.,  $\text{SO}_2$ ,  $\text{NO}_x$ ,  $\text{NH}_3$ , OC, BC, and SOAP) in each month. High-resolution ( $0.01^\circ \times 0.01^\circ$ ) satellite-derived surface PM<sub>2.5</sub> concentrations (van Donkelaar et al., 2021) are

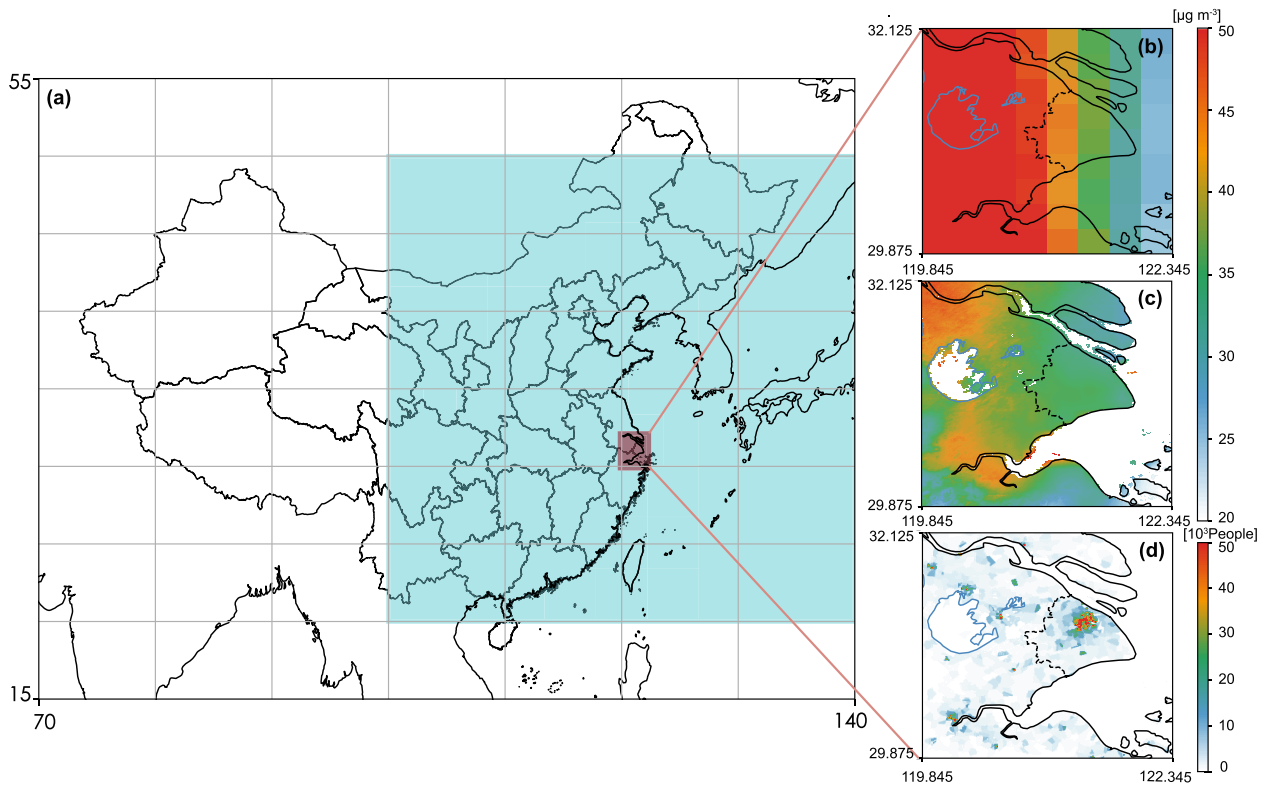


**Fig. 1.** (a) Model domains, distributions of modeled surface-level annual mean PM<sub>2.5</sub> concentrations (b) before and (c) after satellite downscaling and bias correction, as well as (d) the distribution of population in 2019. The outer and inner domains of the nested simulations are shaded in white and blue, respectively. The dash line in (b), (c), and (d) is the boundary of Shanghai considered in the calculation. (For interpretation of the references to colour in this figure legend, the reader is referred to the web version of this article.)

incorporated into the adjoint model to provide better estimates for city-scale PM<sub>2.5</sub> exposure following Nawaz et al. (2021). To capture fine-scale spatial variability of PM<sub>2.5</sub> concentrations, the ratios of satellite-derived surface PM<sub>2.5</sub> concentrations to the same products averaged to our model resolution are applied to the modeled PM<sub>2.5</sub> concentrations from the forward model simulation. Simultaneously, a bias correction is conducted by comparing the simulated PM<sub>2.5</sub> concentrations with the satellite-derived ones in 2019. The receptor function  $J$  is calculated as:

$$J = \frac{\sum_{i \in \text{Shanghai}} (P_i \times \bar{X}_{SAT_i}^{sat_i} \frac{SAT_i}{\bar{X}_i^0})}{\sum_{i \in \text{Shanghai}} P_i} \quad (1)$$

Where  $i$  and  $I$  refer to spatial indexing at the  $0.01^\circ \times 0.01^\circ$  resolution of satellite-derived product and the  $0.25^\circ \times 0.3125^\circ$  resolution of the model, respectively.  $sat_i$  is the satellite-derived annual mean PM<sub>2.5</sub> product, and  $SAT_I$  is the same satellite-based estimate averaged at the model resolution.  $\bar{X}_I$  is annual mean PM<sub>2.5</sub> concentration from the forward model, and  $\bar{X}_I^0$  is the same modeled annual mean PM<sub>2.5</sub>. To capture sub-grid spatial variability of PM<sub>2.5</sub> concentrations, we apply the downscaling ratio  $\frac{sat_i}{SAT_I}$  and rescaling factor  $\frac{SAT_I}{\bar{X}_I^0}$  to the adjoint forcing and treat them as constants during the adjoint calculation. For all the  $sat_i$  values in the grid cell  $I$ , the calculation shares the same denominator (i.e.,  $SAT_I$ ). We apply a mask to identify the area of the city. The shape file is sourced from United Nations Office for the Coordination of Humanitarian Affairs Regional Office for Asia and Pacific (<https://data.humdata.org/dataset/>, last accessed: 29 March 2024).  $P_i$  is the fine resolution population at grid cell  $i$ . The fine-resolution population data, approximately 1 km in scale, is obtained from the Gridded Population of the World version 4 (GPWv4) product (CIESIN, 2018). We employ linear interpolation to estimate the population for the year 2019, utilizing population data available for 2015 and 2020.

The adjoint model computes the linear response (i.e., adjoint sensitivity) of  $J$  to PM<sub>2.5</sub> precursor emission changes within the context of the emission and meteorological conditions specified for the forward model simulation in 2019. The sensitivities are calculated as:

$$\lambda_{s,m,I} = \nabla_{E_{s,m,I}} J = \frac{\partial J}{\partial E_{s,m,I}} \quad (2)$$

Where  $\lambda_{s,m,I}$  is the sensitivity of  $J$  to changes in emissions ( $E_{s,m,I}$ ) of species  $s$  at location  $I$  in month  $m$ . These gradients are calculated at the model resolution ( $0.25^\circ \times 0.3125^\circ$ ). We then consider perturbations in  $J$  owing to changes in emissions resolved at the resolution of the emissions ( $0.1^\circ \times 0.1^\circ$  for HTAPv3 and  $0.25^\circ \times 0.25^\circ$  for MEIC) to better quantify finer-scale features of source attribution. We assume that sensitivities  $\lambda_{s,m,I}$  are constant over each coarse grid box, even though uncertainty may rise due to the loss of sub-grid variability in  $\lambda_{s,m,I}$ . Changes in  $J$  ( $dJ_{s,k,m,d}$ ) caused by emissions ( $dE_{s,k,m,d}$ ) of species  $s$  from sector  $k$  in month  $m$  at emission resolution grid box  $d$  can thus be calculated as:

$$dJ_{s,k,m,d} = \lambda_{s,m,d} dE_{s,k,m,d} \quad (3)$$

where  $\lambda_{s,m,d}$  is the adjoint sensitivity of  $J$  to changes in emissions of species  $s$  in the grid box  $I$  to which the location  $d$  belongs. As discussed in previous analyses (Nawaz et al., 2023; Gu et al., 2023b), Equation (3) may introduce substantial uncertainty under conditions where the response of  $J$  exhibits a high degree of nonlinearity in response to  $dE_{s,k,m,d}$ . To minimize the nonlinear effects, we restrict our analysis to consideration of marginal contributions, i.e., considering a 10 % change in precursor emissions.

To estimate the changes in  $J$  caused by Clean Air Actions during 2013–2019, we recalculate the adjoint sensitivity in 2013 ( $\lambda'_{s,m,d}$ ) by fixing the meteorology in 2019 while changing the anthropogenic

emissions from 2019 to 2013. The adjoint model sensitivity is the tangent linear gradient of the receptor function, the application of which is accurate over a limited range of perturbations (Henze et al., 2007). For secondary components (i.e., NH<sub>3</sub>, NO<sub>x</sub>, SO<sub>2</sub>, and SOA), Equation (3), which is the first-order linear approximation, neglects higher order sensitivities, leading to relatively larger errors when large emission perturbations occur. Therefore, we apply the mean value of the adjoint sensitivities between 2013 and 2019 to account for the nonlinear impacts of emission changes. The corresponding response in  $J$  can be calculated as:

$$dJ_{s,k,m,d} = \frac{1}{2}(\lambda_{s,m,d} + \lambda'_{s,m,d})(E_{s,k,m,d} - E'_{s,k,m,d}) \quad (4)$$

where  $E_{s,k,m,d}$  and  $E'_{s,k,m,d}$  are the anthropogenic emissions of species  $s$  from sector  $k$  in month  $m$  at location  $d$  in 2019 and 2013, respectively.

### 2.3. Health impacts

Premature deaths attributable to chronic PM<sub>2.5</sub> exposure are estimated utilizing the Global Exposure Mortality Model (GEMM; Burnett et al., 2018). Compared to the GBD 2019 study (Murray et al., 2020), GEMM encompasses a broader concentration range to assess the health risks associated with PM<sub>2.5</sub> exposure and generally yields higher estimates of premature deaths. We estimate hazard risk (HR) for non-communicable diseases (NCD) and lower respiratory infections (LRI):

$$HR(z) = e^{\theta T(z)} \quad (5)$$

Here,  $\theta$  is the exposure–response model coefficient,  $z = \max(0, J - 2.4 \mu\text{g m}^{-3})$ , which is the additional PM<sub>2.5</sub> exposure in comparison to the counterfactual PM<sub>2.5</sub> level.  $T(z) = f(z)\omega(z)$  with  $f(z) = \log\left(1 + \frac{z}{\alpha}\right)$ ,

$\omega(z) = 1/(1 + e^{-\frac{z-\mu}{\nu}})$ .  $\alpha$ ,  $\mu$ , and  $\nu$  determine the form of the HR function, which are obtained from Burnett et al. (2018). The number of PM<sub>2.5</sub>-related premature deaths is thus calculated as:

$$O = PB\left(1 - \frac{1}{HR(z)}\right) \quad (6)$$

where  $P$  is the total population in Shanghai;  $B$  is the baseline mortality rate of the health outcome  $O$ . The baseline mortality rate (above 25 years of age) attributed to each outcome in Shanghai is derived (Text S1) according to Zhou et al. (2019) based on the country-level rates obtained from the GBD Results Tool (<https://vizhub.healthdata.org/gbd-results/>, last access: 29 March 2024). Total population and the corresponding proportion of each age group in Shanghai are obtained from the National Bureau of Statistics of China (<https://www.stats.gov.cn/>, last access: 29 March 2024). The impact of a specific source change on PM<sub>2.5</sub>-related health impacts in Shanghai is quantified by calculating the difference in health outcome  $O$  resulting from changes in PM<sub>2.5</sub>-related relative risks. To evaluate the impacts of emission changes, population and the mortality data are fixed to the base year (i.e., 2019) when calculating the changes in the exposure-related health impacts between 2013 and 2019. In Section 3.5, we discuss the uncertainty arising from the health impact estimates in greater detail.

## 3. Results and Discussions

### 3.1. PM<sub>2.5</sub> exposure in Shanghai and model evaluation

Fig. 1b–d displays the distributions of modeled and satellite-derived annual mean PM<sub>2.5</sub> concentrations in Shanghai and its surrounding region, along with the corresponding distribution of population in 2019. As a majority of the population is concentrated in urban areas, the modeled PM<sub>2.5</sub> concentration at the default resolution (Fig. 1b) fails to capture this level of detail, introducing bias in estimating PM<sub>2.5</sub>

exposure. In comparison, the high-resolution satellite-derived PM<sub>2.5</sub> data (Fig. 1c) aligns more closely with the population distribution, providing an approach to adequately characterize the spatial variability of PM<sub>2.5</sub> exposure within the city. Table S1 compares the modeled and satellite-derived annual mean PM<sub>2.5</sub> concentrations and those obtained from in-situ measurements at 10 monitoring sites in Shanghai in 2019, where the observed annual mean PM<sub>2.5</sub> concentrations are derived by averaging hourly measurements from the China National Environmental Monitoring Centre (<https://air.cnemc.cn/>, last access: 9 May 2024). The results suggest that the default forward model outputs inadequately describe the variability of PM<sub>2.5</sub> levels across these monitoring sites, as 8 out of the 10 sites are included in one grid box. By applying satellite downscaling and bias correction, the modeled annual mean PM<sub>2.5</sub> concentration over the 10 monitoring sites decreases from  $39.6 \mu\text{g m}^{-3}$  to  $33.6 \mu\text{g m}^{-3}$ , exhibiting improved consistency with the surface measurements ( $35.9 \mu\text{g m}^{-3}$ ). The normalized mean bias decreases from +10.3 % to –6.4 %. Moreover, the correlation coefficient ( $R$ ) between the modeled and observed PM<sub>2.5</sub> concentrations increases from 0.61 to 0.82, suggesting that city-level PM<sub>2.5</sub> variability is better characterized. There is an exception of a peak near Qingpu, which is not well captured by the satellite observations.

It should be noted that the satellite downscaling and bias correction apply a uniformly scaling factor to all the PM<sub>2.5</sub> components in each  $0.01^\circ \times 0.01^\circ$  grid box. Their ratios in the total PM<sub>2.5</sub> concentrations are still determined by the performance of the forward model. The model's performance in simulating PM<sub>2.5</sub> components can be evaluated by comparing the modeled ratio of each component concentration in the total PM<sub>2.5</sub> concentration to literature studies, displayed in Table S2. With SOA included, the simulated PM<sub>2.5</sub> composition aligns well with literature observations in Shanghai, where nitrate and organic aerosols act as the dominant components accounting for 36.2 % and 23.9 %, respectively of the annual mean PM<sub>2.5</sub> concentration in 2019. In Section 3.5, we discuss the uncertainties from both model PM<sub>2.5</sub> estimates and the estimation of health impacts associated with this exposure. We treat them separately and only consider the latter when determining the uncertainty bounds in following sections, since the covariance between the exposure-related health impact calculation and other types of uncertainties remains to be investigated and the estimation of health impacts is usually the largest source of uncertainty in exposure-associated health assessments (Nawaz, et al., 2021; Gu et al., 2023). In 2019,  $J$  is estimated to be  $33.7 \mu\text{g m}^{-3}$ , which translates into 15,782 (10,467–22,219) premature deaths (NCD + LRI) out of a population of 20.16 million population (above 25 years of age), according to Equation (5) and (6).

### 3.2. Marginal contributions of anthropogenic emissions

To minimize the uncertainty stemming from nonlinear secondary aerosol formation, we analyze marginal contributions, which are changes in  $J$  contributed by a 10 % change in anthropogenic emissions from various sources. Fig. 2a displays the marginal contributions of anthropogenic emissions from Shanghai (SH\_AN), other Chinese provinces (OTH\_CH\_AN), and regions outside of China (nonCH\_AN) within the inner domain in 2019. A 10 % decrease in these emissions can lead to an approximately  $2.6 \mu\text{g m}^{-3}$  decrease in  $J$ , where SH\_AN and OTH\_CH\_AN account for 29.8 % and 63.3 %, respectively, of these decreases. The PM<sub>2.5</sub> changes can translate into 815 (548–1,132) premature deaths (NCD + LRI) in Shanghai, where a 10 % decrease in SH\_AN and OTH\_CH\_AN avoids 241 (161–334) and 511 (345–710) deaths, respectively. Fig. 2b and 2c attribute the marginal contributions of SH\_AN and OTH\_CH\_AN into sectors and species. Changes in NH<sub>3</sub> emissions are found to play dominant roles in marginal changes in  $J$ , making up 64.0 % of the marginal contributions from local emissions and 47.8 % of those from OTH\_CH\_AN. The results are consistent with previous studies (e.g., Bai et al., 2019; Gu et al., 2021a), suggesting that NH<sub>3</sub> emission abatement is crucial in PM<sub>2.5</sub> pollution control in China. Despite the

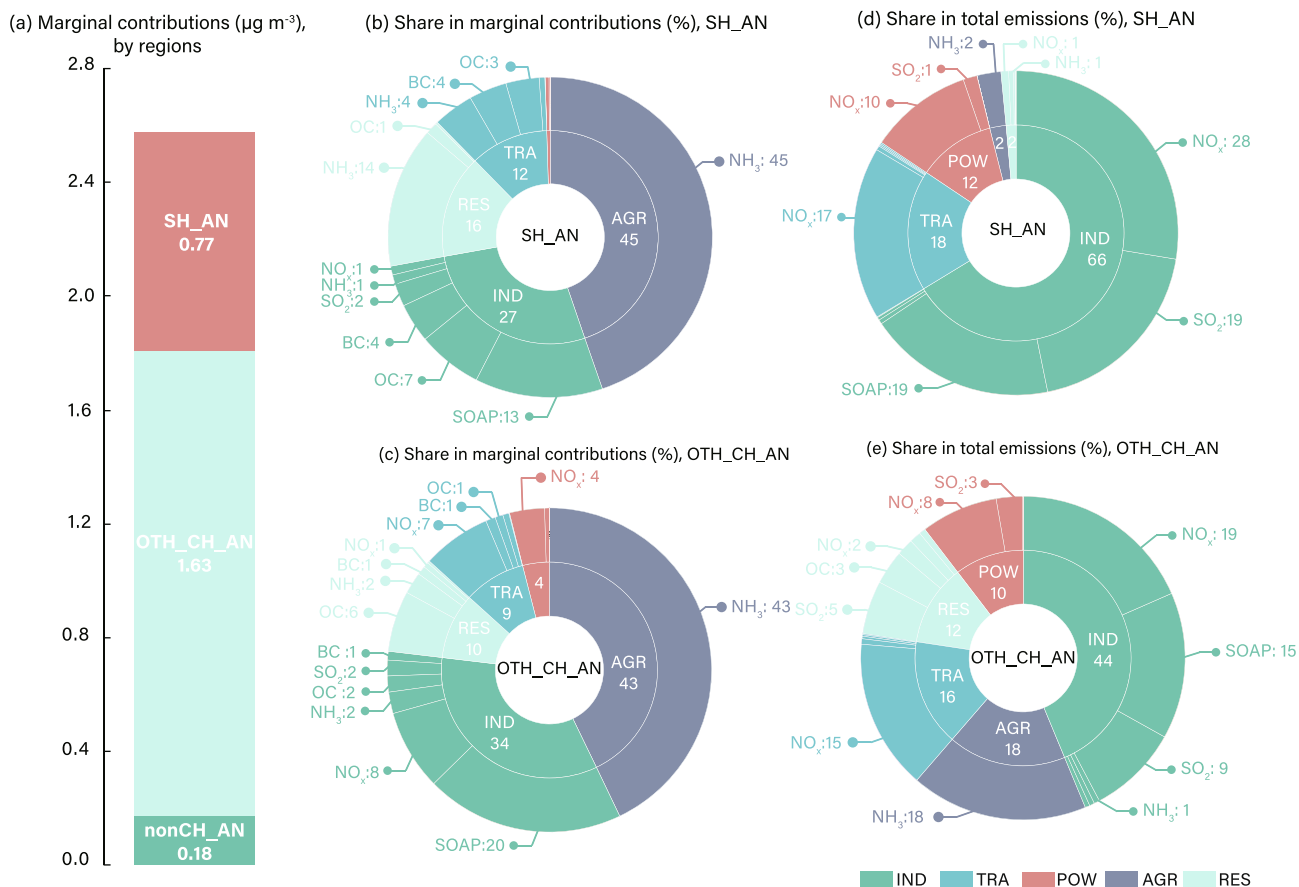


**Fig. 2.** (a) Changes in  $J$  (pop-weighted annual average  $\text{PM}_{2.5}$  in Shanghai) caused by a 10% change in anthropogenic emissions from Shanghai (SH\_AN), other Chinese provinces (OTH\_CH\_AN), and regions outside of China (nonCH\_AN) within the inner domain in 2019. (b) and (c) attribute the marginal contributions of SH\_AN and OTH\_CH\_AN into sectors and species. The inner ring illustrates the marginal contributions across different sectors, while the outer ring provides a more detailed breakdown of each sector's contributions by species. (d) and (e) are the proportions of species emissions in total anthropogenic emissions within and outside Shanghai in China, corresponding to (b) and (c), respectively. We consider five sectors including industry (IND), transportation (TRA), power (POW), residential (RES), and agriculture (AGR) from MEIC emission inventory.

large share of the marginal contributions, total  $\text{NH}_3$  emissions in Shanghai are relatively low, accounting for only 3 % of the mass of local emissions of species that contribute to  $\text{PM}_{2.5}$  mass concentrations. (Fig. 2d). This result suggests a highly sensitive response of  $\text{PM}_{2.5}$

formation to local  $\text{NH}_3$  emission changes under the emission conditions in 2019.

The abundance of free  $\text{NH}_3$  in the sulfate-nitrate-ammonium (SNA) system in the atmosphere can be diagnosed by the molar ratio,  $M$ :

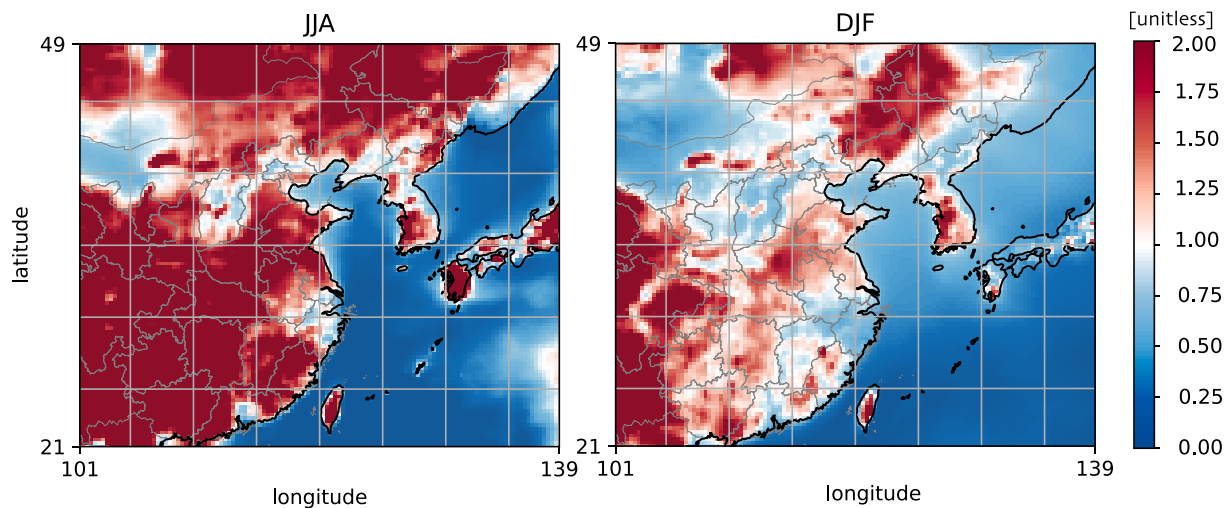


**Fig. 3.** Distributions of seasonal mean molar ratio, defined as  $M = ([\text{NH}_3^T] - 2[\text{SO}_4^{2-}]) / [\text{NO}_3^T]$ , in summer (June to August, JJA) and winter (December to February, DJF) in 2019, where  $[\text{NH}_3^T]$  is the sum of gas-phase  $\text{NH}_3$  and particulate  $\text{NH}_4^+$ , and  $[\text{NO}_3^T]$  is the sum of gas-phase  $\text{HNO}_3$  and particulate  $\text{NO}_3^-$ .

$$M = ([NH_3^T] - 2[SO_4^{2-}]) / [NO_3^T] \quad (7)$$

where  $[NH_3^T]$  is the sum of gas-phase  $NH_3$  and particulate  $NH_4^+$  and  $[NO_3^T]$  is the sum of gas-phase nitric acid ( $HNO_3$ ) and particulate  $NO_3^-$ .  $R > 1$  indicates  $NH_3$  in the atmosphere is in excess while  $R < 1$  suggests nitrate is rich and the formation of ammonium nitrate is limited by  $NH_3$  emissions. As shown in Fig. 3, the value of  $M$  in Shanghai tends to be less than

1 throughout the year, indicating that local  $PM_{2.5}$  formation is significantly limited by ambient  $NH_3$  concentrations. As a result, in addition to agricultural emissions,  $PM_{2.5}$  levels in Shanghai are highly sensitive to changes in  $NH_3$  emissions from local transportation and industrial sectors (Fig. 2b), despite  $NH_3$  emissions accounting for only a small fraction of the total anthropogenic emissions from these sources. For short-term  $PM_{2.5}$  mitigation, local  $NH_3$  emission control is undoubtedly the most

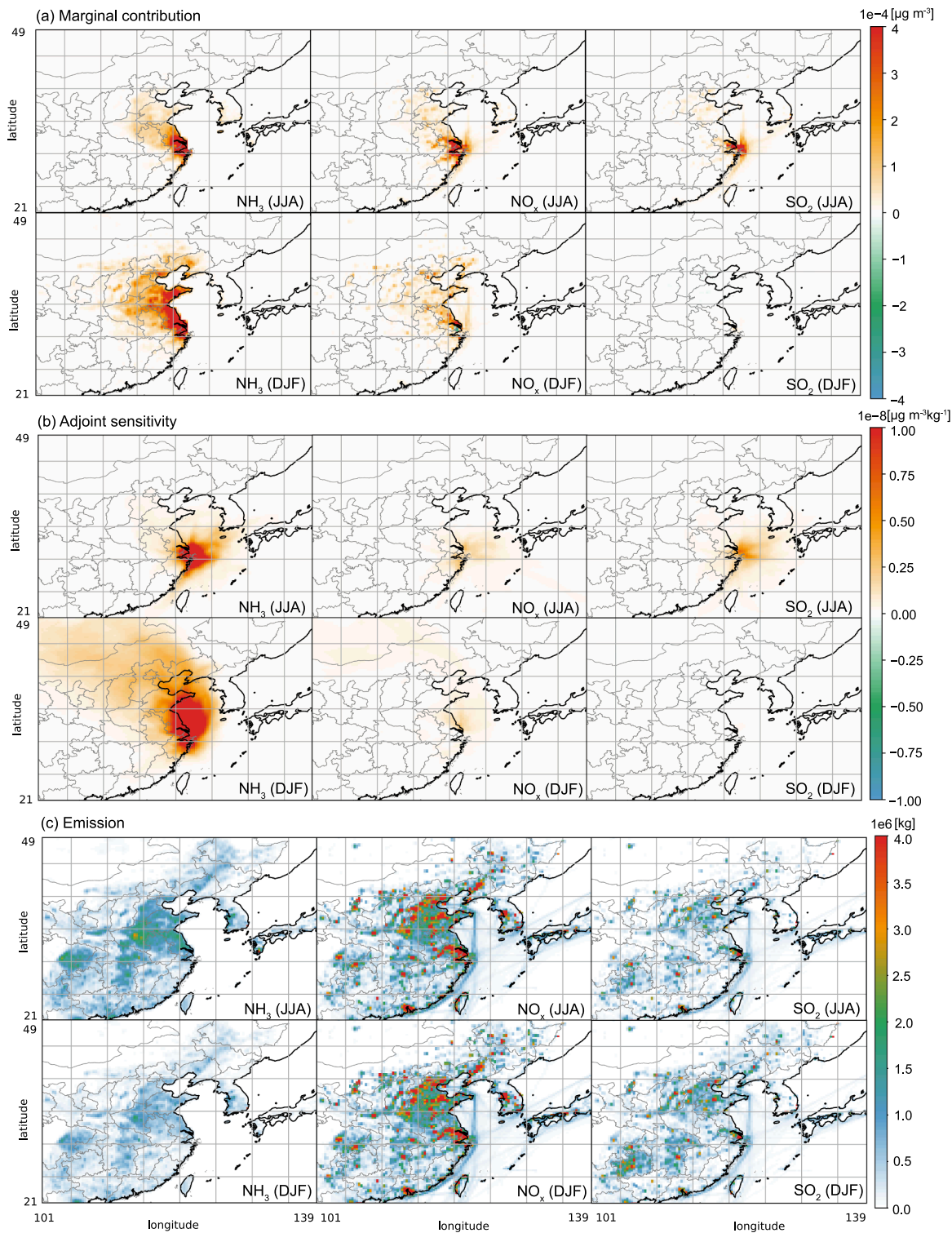


Fig. 4. Distributions of (a) marginal contributions of anthropogenic emissions of  $NH_3$ ,  $NO_x$ , and  $SO_2$  (unit:  $\mu g m^{-3}$ ), (b) mean sensitivity (unit:  $\mu g m^{-3} kg^{-1} box^{-1}$ ) of  $J$  to these species emissions, and (c) total species emissions (unit:  $kg$ ) in summer (JJA) and winter (DJF), respectively. Results for anthropogenic emissions of  $NH_3$ ,  $NO_x$ , and  $SO_2$  are displayed.

effective approach. However, given the low  $\text{NH}_3$  emission levels in Shanghai,  $\text{NO}_x$  and  $\text{SO}_2$  emission abatement within the city remains crucial to balance the ambient SNA ratio, yielding continuous benefits in air quality.  $\text{PM}_{2.5}$  formation outside Shanghai is found to be more constrained by  $\text{NO}_x$  and  $\text{SO}_2$  emissions, where  $M$  is greater than 1 in most provinces during summertime (Fig. 3). As Fig. 2d shows, large  $\text{NH}_3$  emissions, especially those from the agricultural sector, result in substantial free  $\text{NH}_3$  in the atmosphere. In such cases,  $\text{NO}_x$  and  $\text{SO}_2$  emission reductions are effective approaches to reduce  $\text{PM}_{2.5}$  levels in these regions. In winter, as the abundance of free  $\text{NH}_3$  decreases,  $\text{NH}_3$  emission control, on both local and regional scales, can be more effective in reducing  $\text{PM}_{2.5}$  exposure in Shanghai.

Industrial emissions make up 27.3 % and 34.0 % of the marginal contributions of SH\_AN and OTH\_CH\_AN, respectively. SOAP emissions account for 12.7–19.8 % of the marginal contributions of industrial emissions, indicating a crucial part that may have not been counted in previous model-based source apportionment calculations (Zhang et al., 2015; Gu et al., 2021b). An increasing trend in SOA fraction has been observed in Chinese cities in recent years (Gu et al., 2020, 2023c; Huang et al., 2019; Xu et al., 2019). This trend, together with our source attribution results, suggests that controlling emissions of SOAP, for example benzene, toluene, ethylbenzene, and xylenes, are critical for reducing  $\text{PM}_{2.5}$  exposure in Shanghai. Changes in transportation and residential emissions account for 11.7 % and 15.6 %, respectively, of the marginal contributions from SH\_AN (Fig. 2b), and 9.3 % and 9.9 %, respectively of those from OTH\_CH\_AN (Fig. 2c). While the overall proportions are similar, the breakdowns of each sector's share exhibit large differences due to the varying  $\text{PM}_{2.5}$  formation regimes within and outside the city. For local contributions, the transportation and residential parts are mainly associated with anthropogenic emissions of primary carbonaceous aerosols and  $\text{NH}_3$ , respectively. In contrast, for the regional parts, marginal contributions associated with these two sectors are primarily due to changes in  $\text{NO}_x$  and OC emissions, respectively.

### 3.3. Seasonal variations of marginal contributions

Monthly results provide additional insights for formulating effective emission control strategies in different seasons. Fig. 4 presents the marginal contributions of anthropogenic emissions of  $\text{NH}_3$ ,  $\text{NO}_x$ , and  $\text{SO}_2$ , the sensitivity of  $J$  to these species emissions, and the total species emissions in summer and winter in 2019. Similar results for OC, BC, and SOAP are displayed in Fig. S2. Fig. 4a demonstrates that provincial contributions exhibit notable seasonal variations. In summer,  $J$  is primarily affected by changes in emissions from nearby sources, whereas in winter, changes in anthropogenic emissions from distant provinces (e.g., Liaoning, Inner Mongolia) also contribute to  $\text{PM}_{2.5}$  exposure in Shanghai. In addition to local emissions, changes in anthropogenic emissions from Jiangsu and Zhejiang have the largest contributions to  $J$ , making up 34.9 % and 19.0 % of the marginal contributions of OTH\_CH\_AN. The seasonal variations of marginal contributions can be attributed to changes in anthropogenic emissions, atmospheric chemistry, as well as the meteorological conditions. The latter two factors determine the marginal sensitivity (Fig. 4b) of the receptor function (i.e.,  $J$ ), as well as the overall chemical environment, but the sensitivity in any single grid cell is not dependent on the magnitude nor even presence of emissions in that specific location (hence large sensitivities can exist in remote areas or over water).

A 10 % decrease in  $\text{NH}_3$  emissions during wintertime results in larger decreases in  $J$  than those during summertime, even though the wintertime emissions are smaller due to reduced agricultural activities (Zhang et al., 2018). The increased marginal contributions during winter can thus be attributable to the enhanced sensitivity of  $\text{PM}_{2.5}$  formation to  $\text{NH}_3$  emissions (Fig. 4b). The value of  $M$  decreases in winter (Fig. 3) as  $\text{PM}_{2.5}$  formation becomes more sensitive to  $\text{NH}_3$  emission changes due to decreased abundance of free  $\text{NH}_3$  in the atmosphere (Thunis et al.,

2021), and because the meteorological conditions are more favorable for formation of ammonium nitrate. The increased sensitivity of  $J$  to  $\text{NH}_3$  emission changes indicates that  $\text{NH}_3$  emission control can be more efficient in winter; reducing 1 kt  $\text{NH}_3$  emissions within and out of Shanghai would lead to a decrease of  $1.9 \times 10^{-1} \mu\text{g m}^{-3}$  and  $3.5 \times 10^{-4} \mu\text{g m}^{-3}$ , respectively in  $J$  during summer, and a decrease of  $3.2 \times 10^{-1} \mu\text{g m}^{-3}$  and  $1.6 \times 10^{-3} \mu\text{g m}^{-3}$ , respectively in winter.

A 10 % decrease in  $\text{NO}_x$  emission from OTH\_CH\_AN, particularly those from North China, leads to more decreases in  $J$  in winter than summer. As most  $\text{NO}_x$  are emitted by transportation and industrial sources,  $\text{NO}_x$  emissions are relatively constant across the year. The increased marginal contributions in North China can mainly be attributed to more favorable formation conditions of ammonium nitrate (Guo et al., 2018) and long-distance transport. A decrease of 1 kt  $\text{NO}_x$  emissions in Shanghai is estimated to cause a change of  $-5.9 \times 10^{-6} \mu\text{g m}^{-3}$  in  $J$  in winter and a change of  $5.6 \times 10^{-4} \mu\text{g m}^{-3}$  in summer. The negative response of  $\text{PM}_{2.5}$  exposure to  $\text{NO}_x$  emission changes suggests local  $\text{NO}_x$  emission control might lead to adverse impacts on  $\text{PM}_{2.5}$  air quality during wintertime. Similar  $\text{NO}_x$ - $\text{PM}_{2.5}$  relationships have been observed in  $\text{NO}_x$ -rich regions in winter, which is attributed to an increase in the oxidizing capacity of the atmosphere (Huang et al., 2021; Thunis et al., 2021). As ozone ( $\text{O}_3$ ) formation is  $\text{NO}_x$ -saturated in Shanghai (Gu et al., 2024), reducing  $\text{NO}_x$  emissions promotes  $\text{O}_3$  production while weakening  $\text{O}_3$  titration, resulting in increased  $\text{O}_3$  levels in the city. The enhanced oxidizing capacity of the atmosphere is conducive to the production of  $\text{SO}_4^{2-}$  from  $\text{SO}_2$  oxidation and the production of  $\text{NO}_3$  radical via the reaction between  $\text{NO}_2$  and  $\text{O}_3$ , promoting the formation of  $\text{SO}_4^{2-}$  and  $\text{NO}_3^-$  during wintertime (Zhang et al., 2015; Kenagy et al., 2018).

The influence of  $\text{SO}_2$  emission changes on  $J$  is much smaller than those of  $\text{NH}_3$  and  $\text{NO}_x$  on both local and regional scales (Fig. 4b). Compared to emission changes during wintertime,  $\text{SO}_2$  emission changes in summer account for most of the marginal contributions due to the enhanced formation of ammonium sulfate. In 2019, a per-unit (i.e., 1 kt) decrease in  $\text{SO}_2$  emissions within and out of Shanghai can lead to a decrease of  $3.1 \times 10^{-3} \mu\text{g m}^{-3}$  and  $1.2 \times 10^{-4} \mu\text{g m}^{-3}$ , respectively, in  $J$ . In winter, a slightly negative response of  $J$  to  $\text{SO}_2$  emission changes in North China is detected. This is associated with the tradeoff between the formation of ammonium sulfate and ammonium nitrate. Reducing  $\text{SO}_2$  in North China allows more  $\text{NH}_3$  to produce ammonium nitrate during the southward transport of air pollutants and therefore increase the  $\text{PM}_{2.5}$  concentrations in regions where  $\text{PM}_{2.5}$  formation is  $\text{NH}_3$ -limited.

As POM and BC are primary aerosols, their sensitivity patterns are only affected by meteorological changes. During wintertime, as is shown in Fig. S2, the prevalent northerly winds facilitate the long-distance transport of air pollutants, resulting in enhanced response of  $J$  to changes in primary carbonaceous emissions from North China. The increased emissions from the residential sector lead to larger marginal contributions of OC and BC emissions in winter. Since we consider only SOAP emissions from the industrial sector, SOAP emissions exhibit weak seasonal differences. The marginal contributions of SOAP emissions from Shanghai and surrounding regions are enhanced in summer due to the increased OH (Y.F. Gu et al. 2023), while the increased response of  $J$  to changes in SOAP emissions from North China in winter can be mainly attributed to enhanced regional transport (Fig. S2).

Figs. 5 and 6 present the marginal contributions and marginal sensitivities aggregated across species, sectors, provinces and months. Reducing agricultural emissions by 10 % yields more decreases in  $J$  during winter than summer. Given the large  $\text{NH}_3$  sensitivity, controlling agricultural emissions in winter at both local and regional scales turns out to be an effective approach to reduce the population's exposure to  $\text{PM}_{2.5}$  pollution in Shanghai. The marginal contributions of industrial emissions are mainly affected by changes in  $\text{NO}_x$  and SOAP emissions. Even though a per-unit decrease in  $\text{NO}_x$  emissions yield smaller changes in  $J$  than  $\text{NH}_3$ , the marginal contributions of  $\text{NO}_x$  emissions from the

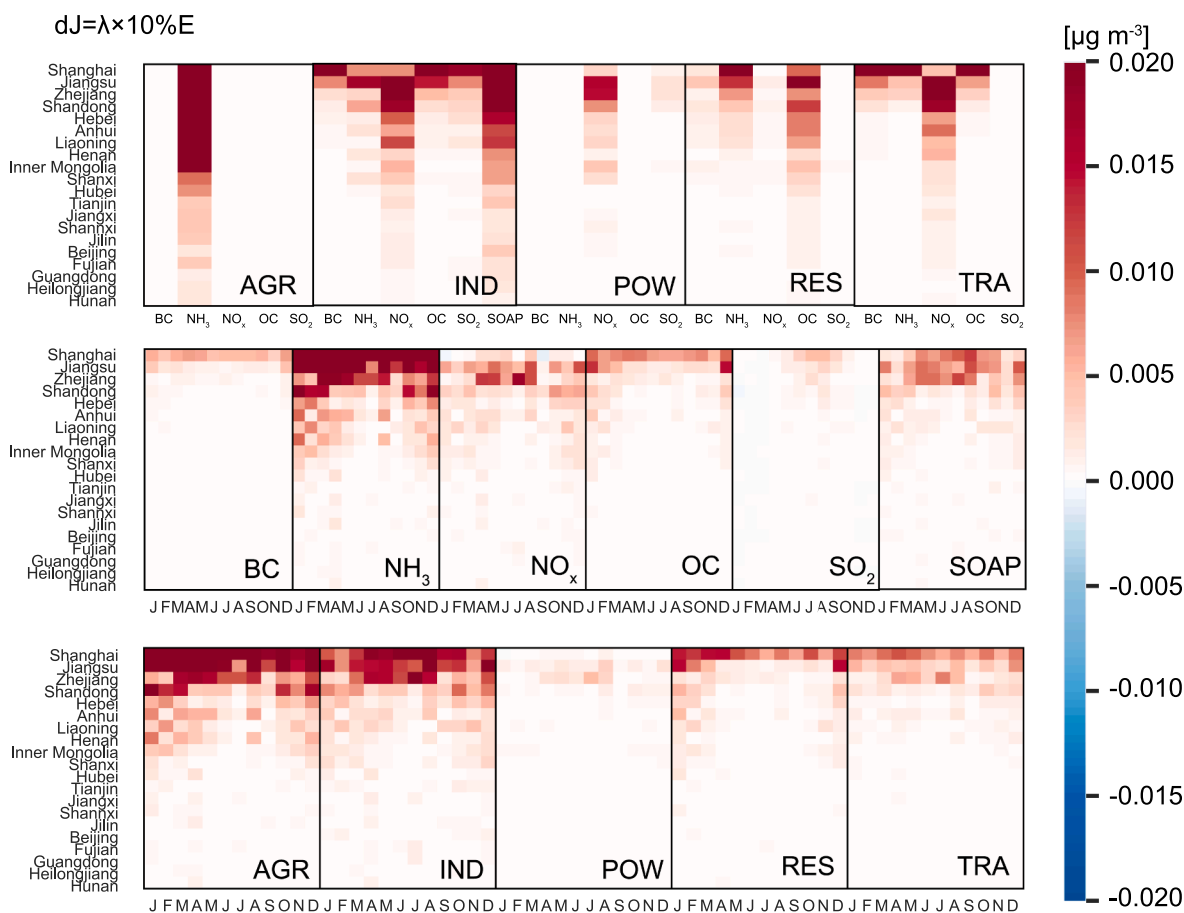


**Fig. 5.** Marginal contributions (unit:  $\mu\text{g m}^{-3}$ ) of anthropogenic emissions aggregated across species, sectors, provinces and months. The results for the top 20 source provinces are shown.

industrial sources remains large due to its high emission levels. As Fig. 6 shows, controlling industrial emissions in nearby provinces (i.e., Jiangsu and Zhejiang) during April to August can lead to more decreases in  $J$ . In addition to the industrial sector, the marginal contributions of transportation and power sectors are also dominated by  $\text{NO}_x$  emission changes. Even though  $\text{SO}_2$  emissions don't act as a key source affecting  $J$ , controlling  $\text{SO}_2$  emissions from industrial and power sectors in Shanghai, Zhejiang and Jiangsu in summer can still benefit  $\text{PM}_{2.5}$  air quality in the city. Wintertime  $\text{SO}_2$  emission reduction in North China may pose challenges for  $J$  due to the negative  $\text{SO}_2$  sensitivity, while these challenges could be mitigated by coordinated  $\text{NH}_3$  and  $\text{NO}_x$  control to reduce the adverse impacts of long-range transport of air pollution. Controlling  $\text{NO}_x$  emissions, especially targeting regional transportation, industrial and power sectors, thus remains a crucial task for coordinated  $\text{PM}_{2.5}$  and  $\text{O}_3$  control for the long-term run. In addition to continental sources,  $J$  is found to be highly sensitive to anthropogenic emission changes from the ocean (Fig. 4b and Fig. S2). Controlling shipping emissions can thus be crucial for reducing the  $\text{PM}_{2.5}$  exposure in Shanghai.

### 3.4. Health benefits of the Clean air Actions

China has implemented a variety of Clean Air Actions to reduce anthropogenic emissions and improve air pollution since 2013. As a result, the annual mean  $\text{PM}_{2.5}$  concentration (satellite-derived) reduced from  $59.86$  to  $33.7 \mu\text{g m}^{-3}$  in Shanghai, translating into  $5,419$  ( $4,520$ – $6,059$ ) premature deaths (NCD + LRI) avoided due to the improved  $\text{PM}_{2.5}$  air quality. To investigate how the  $\text{PM}_{2.5}$ -related health impacts respond to the anthropogenic emission changes, Fig. 7 displays

the changes in the sensitivity of  $J$  to per-unit changes in anthropogenic emissions in terms of species, sectors, and provinces during 2013 to 2019. As POM and BC are primary aerosols, their contributions to  $\text{PM}_{2.5}$  change linearly with their emissions and the magnitude of the sensitivity is only associated with the meteorology. As we keep the meteorological conditions fixed in 2019 when calculating the adjoint sensitivities in 2013, the response of  $J$  in Shanghai to OC and BC emission changes discussed here remains constant. We thus only discuss changes in  $\text{SO}_2$ ,  $\text{NH}_3$ ,  $\text{NO}_x$ , and SOAP sensitivities in the study.

As Fig. 7a shows, the anthropogenic emission changes result in varied sensitivities of  $J$  to per-unit emission changes of  $\text{SO}_2$ ,  $\text{NO}_x$ , and  $\text{NH}_3$ . Since  $\text{NH}_3$  emissions are less regulated compared to those of  $\text{SO}_2$  and  $\text{NO}_x$  (Bai et al., 2019), the amount of free  $\text{NH}_3$  in the atmosphere generally increases, which is shown by increased  $M$  in Fig. S3. As a result,  $J$  becomes less sensitive to  $\text{NH}_3$  emission changes in most continental regions in East China. The reduced  $\text{NH}_3$  sensitivity accompanies increased sensitivity of  $\text{NO}_x$  and  $\text{SO}_2$ , suggesting regional emission control on  $\text{NO}_x$  and  $\text{SO}_2$ , especially  $\text{NO}_x$ , becomes more efficient as anthropogenic emissions are declining. In southern Shanghai and Zhejiang, the amount of free  $\text{NH}_3$  in the atmosphere slightly decreases during the studied period (Fig. S3), making  $\text{PM}_{2.5}$  formation more limited by  $\text{NH}_3$  emissions. The slightly increased  $\text{NH}_3$  sensitivity causes similar  $\text{NH}_3$  emission reductions over these regions tend to yield larger decreases in  $J$  during recent years. Oceanic  $\text{PM}_{2.5}$  formation is highly  $\text{NH}_3$ -limited (Fig. 3), and the response of  $J$  to oceanic  $\text{SO}_2$  and  $\text{NO}_x$  emissions exhibit opposite changes due to the tradeoff between sulfate and nitrate. While the anthropogenic emissions from international shipping and aviation sectors are less regulated (Crippa et al., 2023), increases in oceanic  $\text{SO}_2$  sensitivity suggests that controlling  $\text{SO}_2$

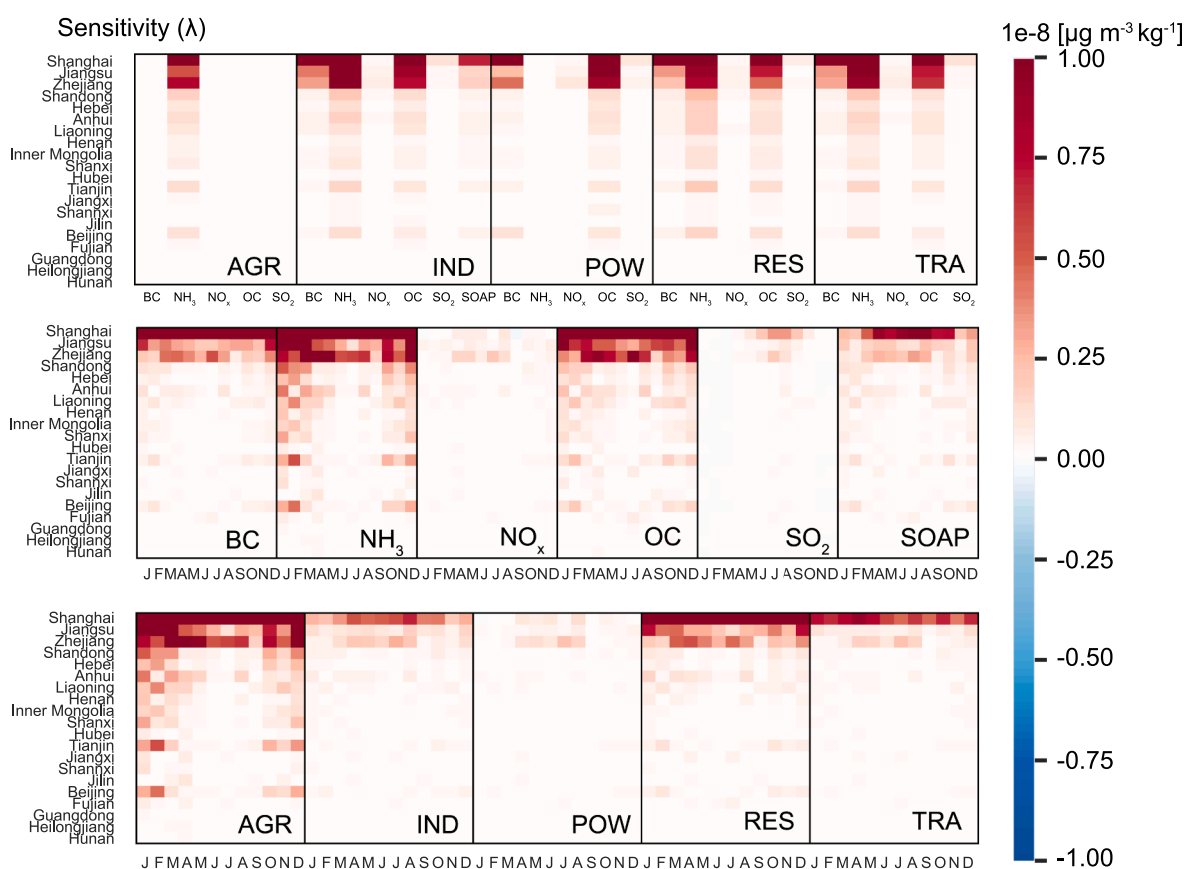


**Fig. 6.** Similar as Fig. 5 but for the sensitivity (unit:  $\mu\text{g m}^{-3}\text{kg}^{-1}$ ) of  $J$  to changes in anthropogenic emissions aggregated across species, sectors, provinces and months.

emissions in these sectors would lead to large improvement in  $\text{PM}_{2.5}$  air quality in Shanghai.

Fig. 7b shows the mean species sensitivity changes in the top 20 source provinces. Apart from  $\text{NH}_3$  emissions from the agricultural and industry sectors, reducing a per-unit local anthropogenic emissions has led to larger decreases in  $J$  in 2019 than 2013 due to regulatory measures. Even though  $\text{PM}_{2.5}$  exposure in Shanghai is more sensitive to changes in  $\text{NH}_3$  emissions than to  $\text{NO}_x$  and  $\text{SO}_2$ , the marginal benefits of reducing local  $\text{NO}_x$  and  $\text{SO}_2$  emissions increase as overall anthropogenic emissions are declining. Continuous regulation of those emissions is thus conducive to achieving long-term air quality goals. Additionally, the marginal benefits caused by a per-unit decrease in local SOAP emissions have increased, suggesting that local VOC emission control can be an effective approach to reducing population's exposure to  $\text{PM}_{2.5}$  pollution in Shanghai. Regional  $\text{NO}_x$  emission control exhibits larger increases in marginal benefits due to emission regulations implemented during 2013–2019. The largest increase is detected in  $\text{NO}_x$  emissions from the power sector in Zhejiang, where a per kt decrease in emissions can yield a  $2.9 \times 10^{-4} \mu\text{g m}^{-3}$  greater reduction in  $J$  in 2019 compared to 2013.

In Fig. 8, we translate the  $\text{PM}_{2.5}$  exposure changes into health benefits in Shanghai, owing to anthropogenic emission changes between 2013 and 2019 in surrounding provinces. Total anthropogenic emission changes in these provinces avoid 3,132 (2,108–4,346) premature deaths attributable to  $\text{PM}_{2.5}$  exposure in Shanghai, in which local emission changes contributed to 43.1 % of these avoided deaths. As a result of the large  $\text{NH}_3$  sensitivity, agricultural emission decreases bring substantial health benefits, where the emission changes in and out of Shanghai help to avoid 541 (364–750) and 551 (371–765) premature deaths, respectively, in the city. Industrial emission changes yield the largest health benefits. In addition to the 564 (380–783) deaths avoided by local emission changes, industrial emission regulations in Jiangsu contribute

significantly to health benefits, helping to prevent 274 (184–380)  $\text{PM}_{2.5}$ -related premature deaths in Shanghai and accounting for 32.5 % of the health benefits from regional industrial emission regulations. Provincial  $\text{NH}_3$  emissions from the transportation sector are found to increase by 0.3–51.0 % during 2013–2019, despite the general decreasing trends in anthropogenic emissions. The increase leads to an additional 26 (18–36) premature deaths in Shanghai. While similar increases (6.1 %) are detected in local  $\text{NO}_x$  emissions from the transportation sector, the related  $\text{PM}_{2.5}$ -related health burden doesn't increase due to the negative response of  $J$  to  $\text{NO}_x$  emission changes during winter. In Shanghai, the rise in  $\text{NH}_3$  emissions from the residential and transportation sectors greatly offsets the health benefits from reductions in other emissions, resulting in a net increase of 2 (1–3) premature deaths due to changes in local transportation emissions. The results highlight the necessity of controlling  $\text{NH}_3$  emissions in the transportation sector to reduce the  $\text{PM}_{2.5}$ -related health burden at the city level, even if the total emissions are not as significant as other pollutants. Similar negative impacts are detected in the residential sector, where the  $\text{NH}_3$  emission increases in Shanghai lead to an additional 29 (20–40) premature deaths within the city. Given the large marginal sensitivity of  $\text{NH}_3$  emissions, reducing  $\text{NH}_3$  emissions on both local and regional scales remains a crucial task for continuously reducing the health risks attributable to  $\text{PM}_{2.5}$  exposure in Shanghai.

### 3.5. Uncertainty and limitations

Uncertainties in estimating  $\text{PM}_{2.5}$  exposure and quantifying its response to emission changes arise from the representativeness of GEOS-Chem's aerosol simulation and the emissions inventories. By incorporating the high-resolution satellite derived surface  $\text{PM}_{2.5}$  products into the adjoint sensitivity calculation and including industrial SOA

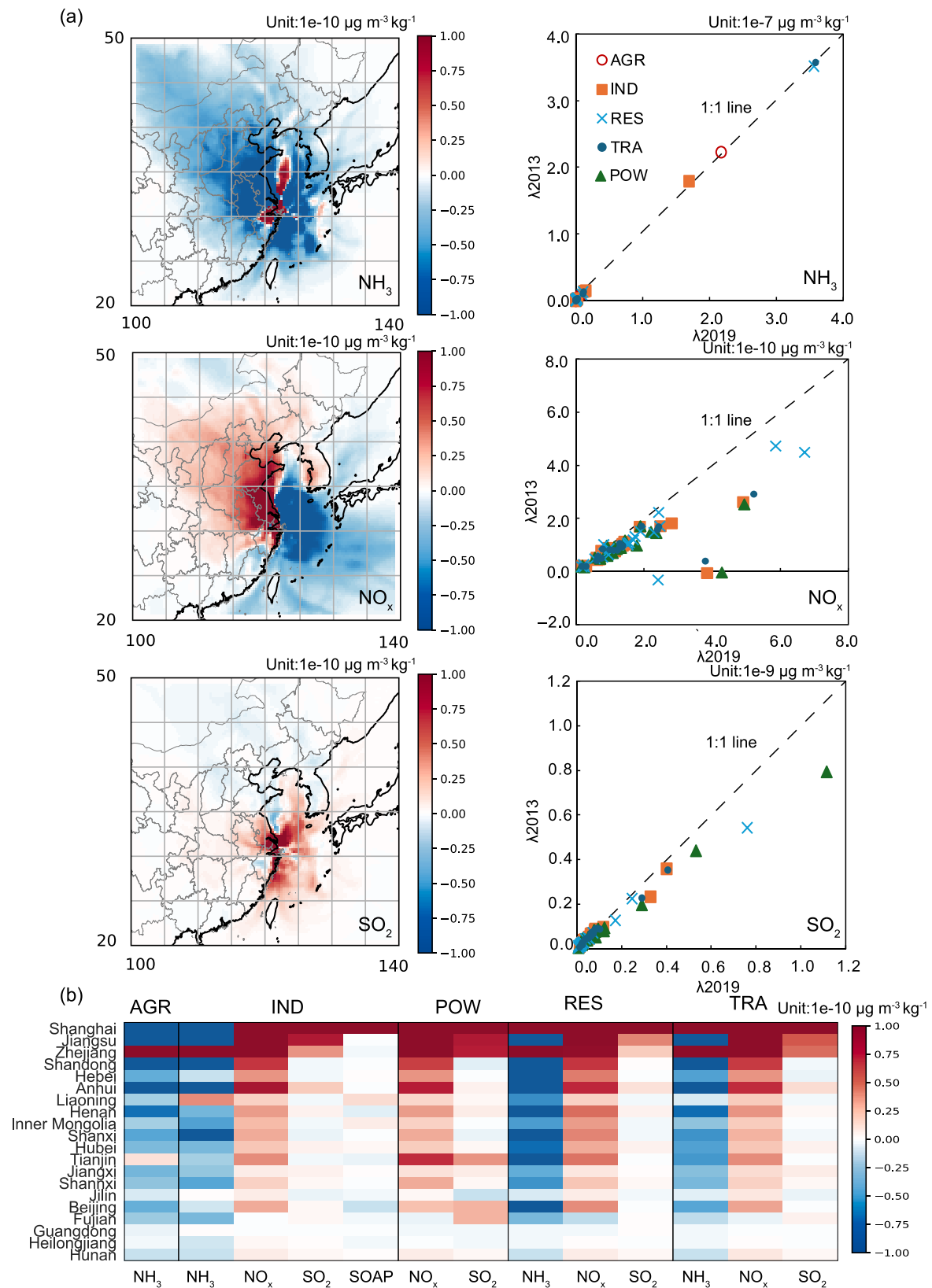


**Fig. 7.** (a) Absolute differences in the sensitivity (left panel, unit:  $\mu\text{g m}^{-3} \text{kg}^{-1}$ ) of  $J$  to per-unit changes in  $\text{NH}_3$ ,  $\text{NO}_x$ , and  $\text{SO}_2$  emissions as a result of the anthropogenic emission changes from 2013 to 2019 in China. The scatter plot (right panel) shows the relationship between the estimated sensitivity in 2013 and 2019 for corresponding species, aggregated across sectors and provinces. The differences in sensitivity aggregated across species, sectors, and provinces, are further displayed in (b). Only results for the top 20 source provinces of  $\text{PM}_{2.5}$  exposure in Shanghai are shown. Compared to the results derived by zero-out experiments, the adjoint sensitivities indicate marginal benefits brought by per-unit decrease in species emissions, which informs the slope of the tangent line of the nonlinear  $\text{PM}_{2.5}$  formation.

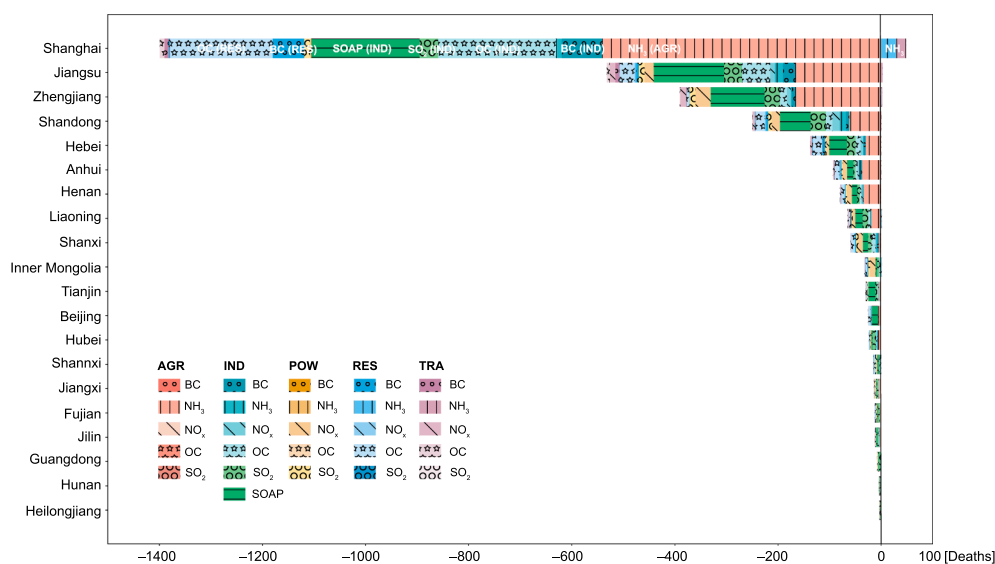


**Fig. 8.** Premature deaths (NCD + LRI) avoided in Shanghai by sectoral and species emission changes in different provinces during 2013 to 2019. Results for provinces where the anthropogenic emission changes cause the top 20 largest decreases in  $PM_{2.5}$ -related premature deaths in Shanghai are shown. The number of health benefits for each bar is listed in Table S3.

components, the uncertainty in the  $PM_{2.5}$  exposure estimate has been greatly reduced. However, SOAP emissions from natural and anthropogenic sources other than the industrial sector are not included. As discussed in Sect. 3.1, the overall mean bias in the model estimated annual mean  $PM_{2.5}$  concentration in Shanghai is approximately  $-2.3 \mu g m^{-3}$ , indicating a slight underestimation of 6.4 % in  $PM_{2.5}$  levels in Shanghai. Attribution of total modeled  $PM_{2.5}$  to sources that do not include biogenic SOA may uniformly overestimate contributions from other species by a similar amount. While the uncertainty in estimating  $PM_{2.5}$  exposure has been reduced, the adjoint model's  $PM_{2.5}$  source-receptor sensitivities still depend on the accuracy of model's chemical and physical schemes, meteorology, and emissions, the effects of which are difficult to isolate. As Table S1 suggested, the overall bias caused by these factors ranges from 0.1 to  $9.8 \mu g m^{-3}$  across different sites in Shanghai, which suggests a 0.3–28.5 % overestimation of exposure and thus health impacts. While estimating the marginal sensitivity changes during 2013–2019 (i.e., Fig. 6), we only account for the impacts of anthropogenic emission changes. Even though the  $PM_{2.5}$  source contribution can be affected by interannual variability in meteorology under actual conditions, we consider our results to be robust since meteorology is reported to only account for 3 % of the  $PM_{2.5}$  changes in Yangtze River Delta region during 2013–2018 (Zhai et al., 2019).

Uncertainties in estimating the health benefits stem from uncertainties in baseline mortality rates, population, and the exposure–response function (ERF). We adopt the 95 % confidence interval from GEMM (Burnett et al., 2018) to calculate the uncertainty bounds of the  $PM_{2.5}$ -related premature deaths (NCD + LRI) in this study. The population data is from the National Bureau of Statistics of China, which we consider to be robust. The uncertainty of our health estimates (both total and provincial) is thus  $\pm 50$  % considering those related to the ERF and baseline mortality. As the local mortality data is not available for Shanghai, we use the country-level mortality rate data from the GBD Results Tool (<https://vizhub.healthdata.org/gbd-results/>, last access: 29 March 2024) and provincial Disability-Adjusted Life Years (DALYs) data from Zhou et al. (2019) to estimate the health outcomes attributable to  $PM_{2.5}$  exposure in the city. As is discussed in Fig. S1 and Text S1, this approach can lead to an additional uncertainty ranging from  $-22.1$  % to  $-5.1$  % in estimating  $PM_{2.5}$ -related premature deaths from different health outcomes in Shanghai. For comparison with the GBD study, GEMM provides a separate ERF for each of the five health outcomes (COD5) that comprise the GBD attributable death estimates: chronic

obstructive pulmonary disorder, ischemic heart disease, LRI, lung cancer, and stroke. In 2019, the annual mean  $PM_{2.5}$  exposure leads to 9,380 (5,018–14,728) premature deaths from COD5 in Shanghai. The improvement in  $PM_{2.5}$  air quality between 2013 and 2019 leads to an avoided 3,662 (2,278–4,577) premature deaths from COD5 within the city. We apply the ERF for NCD and LRI in this study since it comprises a broader set of health outcomes and exhibits smaller uncertainty in premature death estimates.

#### 4. Conclusions

In this study, we use GEOS-Chem and its adjoint to characterize the role of local and distant anthropogenic emissions on health impacts associated with  $PM_{2.5}$  in Shanghai. As of 2019, the  $PM_{2.5}$ -related health burden in Shanghai remains substantial, where the  $PM_{2.5}$  air pollution leads to 15,782 (10,467–22,219) premature deaths from NCD and LRI. Our results suggest that a 10 % decrease in anthropogenic emissions throughout China can avoid 752 (506–1,044)  $PM_{2.5}$ -related premature deaths in Shanghai. Within these benefits, contributions from anthropogenic emissions within Shanghai itself avoid 241 (161–334) premature deaths.

$NH_3$  emissions are found to be a dominant contributor to the  $PM_{2.5}$ -related health impacts in Shanghai. As  $PM_{2.5}$  formation in the city is highly  $NH_3$ -limited, the  $PM_{2.5}$  exposure there is very sensitive to changes in local  $NH_3$  emissions rather than  $NO_x$ . Controlling  $NH_3$  emissions from local sources is thus an effective approach to reduce the population's exposure to  $PM_{2.5}$ . Despite the relatively low levels of emissions, the marginal contributions of  $NH_3$  emissions from local residential, transportation, and industrial sectors are still substantial, accounting for 19.2 % of the marginal contributions associated with local emissions. Even with the existing control policies,  $NH_3$  emissions from local residential and transportation sectors aren't going down in Shanghai. Reducing  $NH_3$  emissions in these sectors, in addition to agricultural emissions, can also be crucial for lowering  $PM_{2.5}$ -related health burden at the city level. Reducing local  $NO_x$  emissions during wintertime increases the  $PM_{2.5}$ -related health risks in Shanghai due to the feedback of  $NO_x$  on oxidant concentrations. However, controlling  $NO_x$  emissions are still justified as the negative impacts decrease as the anthropogenic emissions are declining. Given the high levels of  $NO_x$  emissions, continuous efforts in controlling local  $NO_x$  emissions are still needed for coordinated  $PM_{2.5}$  and  $O_3$  control at the city level.

The effect of regional emission control exhibits seasonal variations due to the varied sensitivity of PM<sub>2.5</sub> exposure in Shanghai to species emissions. Controlling NH<sub>3</sub> emissions is more effective in winter while reducing NO<sub>x</sub> and SO<sub>2</sub> emissions in nearby provinces (e.g., Jiangsu and Zhejiang) brings more health benefits in summer. Additionally, SOAP emissions are found to be crucial for reducing the population's exposure to PM<sub>2.5</sub> pollution, accounting for 12.7–19.8 % of the marginal contributions of industrial sources. As a result of the Clean Air Actions, anthropogenic emissions of most PM<sub>2.5</sub> precursors decrease in China during 2013–2019, which helps avoid 3,132 (2,108–4,346) PM<sub>2.5</sub>-related premature deaths in Shanghai in 2019 relative to 2013. Despite these improvements, anthropogenic emissions from specific sectors (e.g., NH<sub>3</sub> emissions from the transportation sector) still need to be further regulated to safeguard the welfare of Shanghai.

### CRedit authorship contribution statement

**Yixuan Gu:** Writing – review & editing, Writing – original draft, Visualization, Validation, Project administration, Methodology, Investigation, Funding acquisition, Formal analysis, Data curation, Conceptualization. **Daven K. Henze:** Writing – review & editing, Supervision, Resources, Project administration, Methodology, Investigation, Funding acquisition, Formal analysis. **Hong Liao:** Writing – review & editing, Supervision, Resources.

### Declaration of competing interest

The authors declare that they have no known competing financial interests or personal relationships that could have appeared to influence the work reported in this paper.

### Acknowledgement

This work is supported by the National Natural Science Foundation of China (grant no. 42205189) and NASA (grant no. 80NSSC21K1343).

### Appendix A. Supplementary data

Supplementary data to this article can be found online at <https://doi.org/10.1016/j.envint.2025.109259>.

### Data availability

Data will be made available on request.

### References

- Ali, M.A., Huang, Z., Bilal, M., Assiri, M.E., Mhawish, A., Nichol, J.E., De Leeuw, G., Almazroui, M., Wang, Y., Alsubhi, Y., 2023. Long-term PM<sub>2.5</sub> pollution over China: Identification of PM<sub>2.5</sub> pollution hotspots and source contributions. *Sci. Total Environ.* 893, 164871. <https://doi.org/10.1016/j.scitotenv.2023.164871>.
- Bai, Z., Winiwarter, W., Klimont, Z., Velthof, G., Misselbrook, T., Zhao, Z., Jin, X., Oenema, O., Hu, C., Ma, L., 2019. Further improvement of air quality in China needs clear ammonia mitigation target. *Environ. Sci. Technol.* 53, 10542–10544. <https://doi.org/10.1021/acs.est.9b04725>.
- Burnett, R., Chen, H., Szyszkwicz, M., Fann, N., Hubbell, B., Pope, C.A., Apte, J.S., Brauer, M., Cohen, A., Weichenthal, S., Coggins, J., Di, Q., Brunekreef, B., Frostad, J., Lim, S.S., Kan, H., Walker, K.D., Thurston, G.D., Hayes, R.B., Lim, C.C., Turner, M.C., Jerrett, M., Krewski, D., Gapstur, S.M., Diver, W.R., Ostro, B., Goldberg, D., Crouse, D.L., Martin, R.V., Peters, P., Pinault, L., Tjepkema, M., Van Donkelaar, A., Villeneuve, P.J., Miller, A.B., Yin, P., Zhou, M., Wang, L., Janssen, N. A.H., Marra, M., Atkinson, R.W., Tsang, H., Quoc Thach, T., Cannon, J.B., Allen, R. T., Hart, J.E., Laden, F., Cesaroni, G., Forastiere, F., Weinmayr, G., Jaensch, A., Nagel, G., Concin, H., Spadaro, J.V., 2018. Global estimates of mortality associated with long-term exposure to outdoor fine particulate matter. *Proc. Natl. Acad. Sci. USA.* 115, 9592–9597. <https://doi.org/10.1073/pnas.1803222115>.
- Center For International Earth Science Information Network-CIESIN-Columbia University, 2018. Gridded Population of the World, Version 4 (GPWv4): Population Count. Revision 11. <https://doi.org/10.7927/H4JW8BX5>.
- Cohen, A.J., Brauer, M., Burnett, R., Anderson, H.R., Frostad, J., Estep, K., Balakrishnan, K., Brunekreef, B., Dandona, L., Dandona, R., Feigin, V., Freedman, G., Hubbell, B., Jobling, A., Kan, H., Knibbs, L., Liu, Y., Martin, R., Morawska, L.,

- Pope, C.A., Shin, H., Straif, K., Shaddick, G., Thomas, M., Van Dingenen, R., Van Donkelaar, A., Vos, T., Murray, C.J.L., Forouzanfar, M.H., 2017. Estimates and 25-year trends of the global burden of disease attributable to ambient air pollution: an analysis of data from the Global Burden of Diseases Study 2015. *Lancet* 389, 1907–1918. [https://doi.org/10.1016/S0140-6736\(17\)30505-6](https://doi.org/10.1016/S0140-6736(17)30505-6).
- Crippa, M., Guizzardi, D., Butler, T., Keating, T., Wu, R., Kaminski, J., Kuenen, J., Kurokawa, J., Chatani, S., Morikawa, T., Pouliot, G., Racine, J., Moran, M.D., Klimont, Z., Manseau, P.M., Mashayekhi, R., Henderson, B.H., Smith, S.J., Suchyta, H., Muntean, M., Solazzo, E., Banja, M., Schaaf, E., Pagani, F., Woo, J.-H., Kim, J., Monforti-Ferrario, F., Pisoni, E., Zhang, J., Niemi, D., Sassi, M., Ansari, T., Foley, K., 2023. The HTAP v3 emission mosaic: merging regional and global monthly emissions (2000–2018) to support air quality modelling and policies. *Earth Syst. Sci. Data* 15, 2667–2694. <https://doi.org/10.5194/essd-15-2667-2023>.
- Feng, X., Feng, Y., Chen, Y., Cai, J., Li, Q., Chen, J., 2022. Source apportionment of PM<sub>2.5</sub> during haze episodes in Shanghai by the PMF model with PAHs. *J. Clean. Prod.* 330, 129850. <https://doi.org/10.1016/j.jclepro.2021.129850>.
- Gu, Y., Huang, R.J., Li, Y., Duan, J., Chen, Q., Hu, W., Zheng, Y., Lin, C., Ni, H., Dai, W., Cao, J., Liu, Q., Chen, Y., Chen, C., Ovadnevaite, J., Ceburnis, D., O'Dowd, C., 2020. Chemical nature and sources of fine particles in urban Beijing: Seasonality and formation mechanisms. *Environ. Int.* 140, 105732. <https://doi.org/10.1016/j.envint.2020.105732>.
- Gu, Y., Yan, F., Xu, J., Duan, Y., Fu, Q., Qu, Y., Liao, H., 2021b. Mitigated PM<sub>2.5</sub> Changes by the Regional Transport During the COVID-19 Lockdown in Shanghai, China. *Geophys. Res. Lett.* 48. <https://doi.org/10.1029/2021GL092395>.
- Gu, Y., Henze, D.K., Nawaz, M.O., Cao, H., Wagner, U.J., 2023a. Sources of PM<sub>2.5</sub>-Associated Health Risks in Europe and Corresponding Emission-Induced Changes During 2005–2015. *GeoHealth* 7. <https://doi.org/10.1029/2022GH000767>.
- Gu, Y., Henze, D.K., Nawaz, M.O., Wagner, U.J., 2023b. Response of the ozone-related health burden in Europe to changes in local anthropogenic emissions of ozone precursors. *Environ. Res. Lett.* 18, 114034. <https://doi.org/10.1088/1748-9326/ad0167>.
- Gu, Y., Huang, R.-J., Duan, J., Xu, W., Lin, C., Zhong, H., Wang, Y., Ni, H., Liu, Q., Xu, R., Wang, L., Li, Y.J., 2023c. Multiple pathways for the formation of secondary organic aerosol in the North China Plain in summer. *Atmos. Chem. Phys.* 23, 5419–5433. <https://doi.org/10.5194/acp-23-5419-2023>.
- Gu, Y., Yan, F., Xu, J., Pan, L., Yin, C., Gao, W., Liao, H., 2024. Observational evidence of the vertical exchange of ozone within the urban planetary boundary layer in Shanghai, China. *Atmosphere* 15, 248. <https://doi.org/10.3390/atmos15030248>.
- Gu, B., Zhang, L., Van Dingenen, R., Vieno, M., Van Grinsven, H.J., Zhang, X., Zhang, S., Chen, Y., Wang, S., Ren, C., Rao, S., Holland, M., Winiwarter, W., Chen, D., Xu, J., Sutton, M.A., 2021a. Abating ammonia is more cost-effective than nitrogen oxides for mitigating PM<sub>2.5</sub> air pollution. *Science* 374, 758–762. <https://doi.org/10.1126/science.abf8623>.
- Guenther, A., Karl, T., Harley, P., Wiedinmyer, C., Palmer, P.I., Geron, C., 2006. Estimates of global terrestrial isoprene emissions using MEGAN (Model of Emissions of Gases and Aerosols from Nature). *Atmos. Chem. Phys.* 6, 3181–3210. <https://doi.org/10.5194/acp-6-3181-2006>.
- Guo, H., Otjes, R., Schlag, P., Kiendler-Scharr, A., Nenes, A., Weber, R.J., 2018. Effectiveness of ammonia reduction on control of fine particulate nitrate. *Atmos. Chem. Phys.* 18, 12241–12256. <https://doi.org/10.5194/acp-18-12241-2018>.
- Hakami, A., Henze, D.K., Seinfeld, J.H., Singh, K., Sandu, A., Kim, S., Byun, Li Q., 2007. The Adjoint of CMAQ. *Environ. Sci. Technol.* 41, 7807–7817. <https://doi.org/10.1021/es070944p>.
- Henze, D.K., Hakami, A., Seinfeld, J.H., 2007. Development of the adjoint of GEOS-Chem. *Atmos. Chem. Phys.* 7, 2413–2433. <https://doi.org/10.5194/acp-7-2413-2007>.
- Henze, D.K., Seinfeld, J.H., Shindell, D.T., 2009. Inverse modeling and mapping US air quality influences of inorganic PM<sub>2.5</sub> precursor emissions using the adjoint of GEOS-Chem. *Atmos. Chem. Phys.* 9, 5877–5903. <https://doi.org/10.5194/acp-9-5877-2009>.
- Hu, W., Zhao, Y., Lu, N., Wang, X., Zheng, B., Henze, D.K., Zhang, L., Fu, T.-M., Zhai, S., 2024. Changing Responses of PM<sub>2.5</sub> and Ozone to Source Emissions in the Yangtze River Delta Using the Adjoint Model. *Environ. Sci. Technol.* 58, 628–638. <https://doi.org/10.1021/acs.est.3c05049>.
- Huang, G., Brook, R., Crippa, M., Janssens-Maenhout, G., Schieberle, C., Dore, C., Guizzardi, D., Muntean, M., Schaaf, E., Friedrich, R., 2017. Speciation of anthropogenic emissions of non-methane volatile organic compounds: A global gridded data set for 1970–2012. *Atmos. Chem. Phys.* 17 (12), 7683–7701. <https://doi.org/10.5194/acp-17-7683-2017>.
- Huang, X., Ding, A., Gao, J., Zheng, B., Zhou, D., Qi, X., Tang, R., Wang, J., Ren, C., Nie, W., Chi, X., Xu, Z., Chen, L., Li, Y., Che, F., Pang, N., Wang, H., Tong, D., Qin, W., Cheng, W., Liu, W., Fu, Q., Liu, B., Chai, F., Davis, S.J., Zhang, Q., He, K., 2021. Enhanced secondary pollution offset reduction of primary emissions during COVID-19 lockdown in China. *Natl. Sci. Rev.* 8, nraa137. <https://doi.org/10.1093/nsr/nraa137>.
- Huang, R.-J., Wang, Y., Cao, J., Lin, C., Duan, J., Chen, Q., Li, Y., Gu, Y., Yan, J., Xu, W., Fröhlich, R., Canonaco, F., Bozzetti, C., Ovadnevaite, J., Ceburnis, D., Canagaratna, M.R., Jayne, J., Worsnop, D.R., El-Haddad, I., Prévôt, A.S.H., O'Dowd, C.D., 2019. Primary emissions versus secondary formation of fine particulate matter in the most polluted city (Shijiazhuang) in North China. *Atmos. Chem. Phys.* 19, 2283–2298. <https://doi.org/10.5194/acp-19-2283-2019>.
- Hudman, R.C., Moore, N.E., Mebust, A.K., Martin, R.V., Russell, A.R., Valin, L.C., Cohen, R.C., 2012. Steps towards a mechanistic model of global soil nitric oxide emissions: implementation and space based-constraints. *Atmos. Chem. Phys.* 12, 7779–7795. <https://doi.org/10.5194/acp-12-7779-2012>.

- Institute for Health Metrics and Evaluation (IHME). Findings from the Global Burden of Disease Study 2017. Seattle, WA: IHME, 2018.
- IQAir, 2023. 2023 World Air Quality Report: Region & City PM<sub>2.5</sub> Ranking. [https://www.iqair.com/dl/2023\\_World\\_Air\\_Quality\\_Report.pdf](https://www.iqair.com/dl/2023_World_Air_Quality_Report.pdf) (accessed 2 August 2024).
- Kenagy, H.S., Sparks, T.L., Ebben, C.J., Wooldridge, P.J., Lopez-Hilfiker, F.D., Lee, B.H., Thornton, J.A., McDuffie, E.E., Fibiger, D.L., Brown, S.S., Montzka, D.D., Weinheimer, A.J., Schroder, J.C., Campuzano-Jost, P., Day, D.A., Jimenez, J.L., Dibb, J.E., Campos, T., Shah, V., Jaeglé, L., Cohen, R.C., 2018. NO<sub>x</sub> Lifetime and NO<sub>y</sub> Partitioning During WINTER. *JGR Atmospheres* 123, 9813–9827. <https://doi.org/10.1029/2018JD028736>.
- Lelieveld, J., Evans, J.S., Fnais, M., Giannadaki, D., Pozzer, A., 2015. The contribution of outdoor air pollution sources to premature mortality on a global scale. *Nature* 525, 367–371. <https://doi.org/10.1038/nature15371>.
- Li, Y., Henze, D.K., Jack, D., Kinney, P.L., 2016b. The influence of air quality model resolution on health impact assessment for fine particulate matter and its components. *Air Qual Atmos Health* 9, 51–68. <https://doi.org/10.1007/s11869-015-0321-z>.
- Li, K., Liao, H., Zhu, J., Moch, J.M., 2016a. Implications of RCP emissions on future PM<sub>2.5</sub> air quality and direct radiative forcing over China. *JGR Atmospheres* 121. <https://doi.org/10.1002/2016JD025623>.
- Li, Y., Liu, B., Xue, Z., Zhang, Y., Sun, X., Song, C., Dai, Q., Fu, R., Tai, Y., Gao, J., Zheng, Y., Feng, Y., 2020. Chemical characteristics and source apportionment of PM<sub>2.5</sub> using PMF modelling coupled with 1-hr resolution online air pollutant dataset for Linfen, China. *Environ. Pollut.* 263, 114532. <https://doi.org/10.1016/j.envpol.2020.114532>.
- Liu, H., Liu, J., Li, M., Gou, P., Cheng, Y., 2022. Assessing the evolution of PM<sub>2.5</sub> and related health impacts resulting from air quality policies in China. *Environ. Impact Assess. Rev.* 93, 106727. <https://doi.org/10.1016/j.eiar.2021.106727>.
- Lu, X., Lin, C., Li, W., Chen, Y., Huang, Y., Fung, J.C.H., Lau, A.K.H., 2019. Analysis of the adverse health effects of PM<sub>2.5</sub> from 2001 to 2017 in China and the role of urbanization in aggravating the health burden. *Sci. Total Environ.* 652, 683–695. <https://doi.org/10.1016/j.scitotenv.2018.10.140>.
- Mao, Y.-H., Zhao, X., Liao, H., Zhao, D., Tian, P., Henze, D.K., Cao, H., Zhang, L., Li, J., Li, J., Ran, L., Zhang, Q., 2020. Sources of black carbon during severe haze events in the Beijing–Tianjin–Hebei region using the adjoint method. *Sci. Total Environ.* 740, 140149. <https://doi.org/10.1016/j.scitotenv.2020.140149>.
- Murray, C.J.L., Aravkin, A.Y., Zheng, P., Abbafati, C., Abbas, K.M., Abbasi-Kangevari, M., Abd-Allah, F., Abdelalim, A., Abdollahi, M., Abdollahpour, I., Abegaz, K.H., Abolhassani, H., Aboyans, V., Abreu, L.G., Abrego, M.R.M., Abualhasan, A., Abu-Raddad, L.J., Abushouk, A.I., Adabi, M., Adekanmbi, V., Adeoye, A.M., Adetokunbo, O.O., Adham, D., et al., 2020. Global burden of 87 risk factors in 204 countries and territories, 1990–2019: a systematic analysis for the Global Burden of Disease Study 2019. *Lancet* 396, 1223–1249. [https://doi.org/10.1016/S0140-6736\(20\)30752-2](https://doi.org/10.1016/S0140-6736(20)30752-2).
- Murray, L.T., Jacob, D.J., Logan, J.A., Hudman, R.C., Koshak, W.J., 2012. Optimized regional and interannual variability of lightning in a global chemical transport model constrained by LIS/OTD satellite data. *J. Geophys. Res.* 117. <https://doi.org/10.1029/2012JD017934>.
- Nault, B.A., Jo, D.S., McDonald, B.C., Campuzano-Jost, P., Day, D.A., Hu, W., Schroder, J.C., Allan, J., Blake, D.R., Canagaratna, M.R., Coe, H., Coggon, M.M., DeCarlo, P.F., Diskin, G.S., Dunmore, R., Flocke, F., Fried, A., Gilman, J.B., Gkatzelis, G., Hamilton, J.F., Hanisco, T.F., Hayes, P.L., Henze, D.K., Hodzic, A., Hopkins, J., Hu, M., Huey, L.G., Jobson, B.T., Kuster, W.C., Lewis, A., Li, M., Liao, J., Nawaz, M.O., Pollack, I.B., Peischl, J., Rappenglück, B., Reeves, C.E., Richter, D., Roberts, J.M., Ryerson, T.B., Shao, M., Sommers, J.M., Walega, J., Warneke, C., Weibring, P., Wolfe, G.M., Young, D.E., Yuan, B., Zhang, Q., De Gouw, J.A., Jimenez, J.L., 2021. Secondary organic aerosols from anthropogenic volatile organic compounds contribute substantially to air pollution mortality. *Atmos. Chem. Phys.* 21, 11201–11224. <https://doi.org/10.5194/acp-21-11201-2021>.
- Nawaz, M.O., Henze, D.K., 2020. Premature Deaths in Brazil Associated With Long-Term Exposure to PM<sub>2.5</sub> From Amazon Fires Between 2016 and 2019. *GeoHealth* 4, e2020GH000268. <https://doi.org/10.1029/2020GH000268>.
- Nawaz, M.O., Henze, D.K., Harkins, C., Cao, H., Nault, B., Jo, D., Jimenez, J., Anenberg, S.C., Goldberg, D.L., Qu, Z., 2021. Impacts of sectoral, regional, species, and day-specific emissions on air pollution and public health in Washington, DC. *Elementa: Sci. Anthropocene* 9, 00043. <https://doi.org/10.1525/elementa.2021.00043>.
- Nawaz, M.O., Henze, D.K., Anenberg, S.C., Braun, C., Miller, J., Pronk, E., 2023. A Source Apportionment and Emission Scenario Assessment of PM<sub>2.5</sub> - and O<sub>3</sub> -Related Health Impacts in G20 Countries. *GeoHealth* 7. <https://doi.org/10.1029/2022GH000713>.
- Philip, S., Martin, R.V., Pierce, J.R., Jimenez, J.L., Zhang, Q., Canagaratna, M.R., Spracklen, D.V., Nowlan, C.R., Lamsal, L.N., Cooper, M.J., Krotkov, N.A., 2014. Spatially and seasonally resolved estimate of the ratio of organic mass to organic carbon. *Atmos. Environ.* 87, 34–40. <https://doi.org/10.1016/j.atmosenv.2013.11.065>.
- Ping, L., Wang, Y., Lu, Y., Lee, L.-C., Liang, C., 2023. Tracing the sources of PM<sub>2.5</sub>-related health burden in China. *Environ. Pollut.* 327, 121544. <https://doi.org/10.1016/j.envpol.2023.121544>.
- Punger, E.M., West, J.J., 2013. The effect of grid resolution on estimates of the burden of ozone and fine particulate matter on premature mortality in the USA. *Air Qual Atmos Health* 6, 563–573. <https://doi.org/10.1007/s11869-013-0197-8>.
- Shanghai Municipal Bureau of Statistics, 2023. Shanghai Statistical Yearbook 2022. <https://tjj.sh.gov.cn/tjgb/20230317/6bb2cf0811ab41eb8ae397c8f8577e00.html> (accessed 16 July 2024).
- Shi, W., Bi, J., Liu, R., Liu, M., Ma, Z., 2021. Decrease in the chronic health effects from PM<sub>2.5</sub> during the 13th Five-Year Plan in China: Impacts of air pollution control policies. *J. Clean. Prod.* 317, 128433. <https://doi.org/10.1016/j.jclepro.2021.128433>.
- Thunis, P., Clappier, A., Beekmann, M., Putaud, J.P., Cuvelier, C., Madrazo, J., De Meij, A., 2021. Non-linear response of PM<sub>2.5</sub> to changes in NO<sub>x</sub> and NH<sub>3</sub> emissions in the Po basin (Italy): consequences for air quality plans. *Atmos. Chem. Phys.* 21, 9309–9327. <https://doi.org/10.5194/acp-21-9309-2021>.
- Van Der Werf, G.R., Randerson, J.T., Giglio, L., Collatz, G.J., Mu, M., Kasibhatla, P.S., Morton, D.C., DeFries, R.S., Jin, Y., Van Leeuwen, T.T., 2010. Global fire emissions and the contribution of deforestation, savanna, forest, agricultural, and peat fires (1997–2009). *Atmos. Chem. Phys.* 10, 11707–11735. <https://doi.org/10.5194/acp-10-11707-2010>.
- Van Donkelaar, A., Hammer, M.S., Bindle, L., Brauer, M., Brook, J.R., Garay, M.J., Hsu, N.C., Kalashnikova, O.V., Kahn, R.A., Lee, C., Levy, R.C., Lyapustin, A., Sayer, A.M., Martin, R.V., 2021. Monthly Global Estimates of Fine Particulate Matter and Their Uncertainty. *Environ. Sci. Technol.* 55, 15287–15300. <https://doi.org/10.1021/acs.est.1c05309>.
- Wang, S., Zhu, L., Henze, D.K., Fu, T.-M., Zhang, L., Wang, X., Fan, S., Chen, Y., 2022. An Effective Mitigation Strategy for O<sub>3</sub> and PM<sub>2.5</sub> Co-Pollution in the Pearl River Delta, China Based on the Adjoint Sensitivities. *SSRN J.* <https://doi.org/10.2139/ssrn.4074753>.
- Xiao, Q., Geng, G., Xue, T., Liu, S., Cai, C., He, K., Zhang, Q., 2022. Tracking PM<sub>2.5</sub> and O<sub>3</sub> Pollution and the Related Health Burden in China 2013–2020. *Environ. Sci. Technol.* 56, 6922–6932. <https://doi.org/10.1021/acs.est.1c04548>.
- Xu, W., Sun, Y., Wang, Q., Zhao, J., Wang, J., Ge, X., Xie, C., Zhou, W., Du, W., Li, J., Fu, P., Wang, Z., Worsnop, D.R., Coe, H., 2019. Changes in Aerosol Chemistry From 2014 to 2016 in Winter in Beijing: Insights From High-Resolution Aerosol Mass Spectrometry. *JGR Atmospheres* 124, 1132–1147. <https://doi.org/10.1029/2018JD029245>.
- Zender, C.S., Bian, H., Newman, D., 2003. Mineral Dust Entrainment and Deposition (DEAD) model: Description and 1990s dust climatology. *J. Geophys. Res.* 108. <https://doi.org/10.1029/2002JD002775>.
- Zhai, S., Jacob, D.J., Wang, X., Shen, L., Li, K., Zhang, Y., Gui, K., Zhao, T., Liao, H., 2019. Fine particulate matter (PM<sub>2.5</sub>) trends in China, 2013–2018: separating contributions from anthropogenic emissions and meteorology. *Atmos. Chem. Phys.* 19, 11031–11041. <https://doi.org/10.5194/acp-19-11031-2019>.
- Zhang, L., Liu, L., Zhao, Y., Gong, S., Zhang, X., Henze, D.K., Capps, S.L., Fu, T.-M., Zhang, Q., Wang, Y., 2015. Source attribution of particulate matter pollution over North China with the adjoint method. *Environ. Res. Lett.* 10, 084011. <https://doi.org/10.1088/1748-9326/10/8/084011>.
- Zhang, L., Shao, J., Lu, X., Zhao, Y., Hu, Y., Henze, D.K., Liao, H., Gong, S., Zhang, Q., 2016. Sources and Processes Affecting Fine Particulate Matter Pollution over North China: An Adjoint Analysis of the Beijing APEC Period. *Environ. Sci. Technol.* 50, 8731–8740. <https://doi.org/10.1021/acs.est.6b03010>.
- Zhang, L., Chen, Y., Zhao, Y., Henze, D.K., Zhu, L., Song, Y., Paulot, F., Liu, X., Pan, Y., Lin, Y., Huang, B., 2018. Agricultural ammonia emissions in China: reconciling bottom-up and top-down estimates. *Atmos. Chem. Phys.* 18, 339–355. <https://doi.org/10.5194/acp-18-339-2018>.
- Zhao, H., Geng, G., Zhang, Q., Davis, S.J., Li, X., Liu, Y., Peng, L., Li, M., Zheng, B., Huo, H., Zhang, L., Henze, D.K., Mi, Z., Liu, Z., Guan, D., He, K., 2019. Inequality of household consumption and air pollution-related deaths in China. *Nat Commun* 10, 4337. <https://doi.org/10.1038/s41467-019-12254-x>.
- Zheng, S., Schlink, U., Ho, K., Singh, R.P., Pozzer, A., 2021. Spatial Distribution of PM<sub>2.5</sub>-Related Premature Mortality in China. *GeoHealth* 5. <https://doi.org/10.1029/2021GH000532>.
- Zhou, M., Wang, H., Zeng, X., Yin, P., Zhu, J., Chen, W., Li, X., Wang, L., Wang, L., Liu, Y., Liu, J., Zhang, M., Qi, J., Yu, S., Afshin, A., Gakidou, E., Glenn, S., Krish, V.S., Miller-Petrie, M.K., Mountjoy-Venning, W.C., Mullany, E.C., Redford, S.B., Liu, H., Naghavi, M., Hay, S.I., Wang, L., Murray, C.J.L., Liang, X., 2019. Mortality, morbidity, and risk factors in China and its provinces, 1990–2017: a systematic analysis for the Global Burden of Disease Study 2017. *Lancet* 394, 1145–1158. [https://doi.org/10.1016/S0140-6736\(19\)30427-1](https://doi.org/10.1016/S0140-6736(19)30427-1).